β-hydroxybutyrate Prevents Cellular Senescence and Apoptosis in Cisplatin-Induced Acute Kidney Injury

계 명 대 학 교 대 학 원

의 학 과

김 미 경

지도교수 하 은 영

2 0 2 3 년 8 월

β-hydroxybutyrate Prevents Cellular Senescence and Apoptosis in Cisplatin-Induced Acute Kidney Injury

지도교수   하   은   영

이 논문을 박사학위 논문으로 제출함

2 0 2 3 년   8 월

계 명 대 학 교 대 학 원

의학과 생화학 전공

김   미   경

김미경의 박사학위 논문을 인준함

주 심 서 지 혜

부 심 하 은 영

부 심 신 소 진

부 심 김 진 영

부 심 하 태 경

계 명 대 학 교 대 학 원

2 0 2 3 년 8 월

Table of Contents

List of Table

List of Figures

1. Introduction

Cisplatin (CP) is a platinum-based chemotherapeutic agent. It is commonly used to treat diverse types of solid cancers. Although CP is a powerful chemotherapeutic agent, it has significant side effects. Common side effects of CP treatment include nephrotoxicity (kidney damage), gastrointestinal toxicity (nausea, vomiting, and diarrhea), ototoxicity (hearing loss), and myelosuppression (reduced blood cell production), with nephrotoxicity being the most serious and limiting one (1‑3). Accumulation of CP in the kidney is the cause of CP-induced nephrotoxicity, which results in tubular injury associated with cell death, inflammation, vascular damage, and oxidative and endoplasmic reticulum stress, ultimately leading to acute kidney injury (AKI) (4‑12).

Signs of AKI include an increase in serum creatinine (SCr) or blood urea nitrogen (BUN). Currently, there is no treatment or method that effectively prevents CP-induced AKI (13,14). AKI is caused by the production of reactive oxygen species (ROS), activation of apoptotic and senescence pathways, and inhibition of cell proliferation (12). ROS are considered to be a major cause of CP-induced AKI, so protecting the kidney from ROS could prevent structural as well as functional damages (15,16).

ROS play a crucial function in regulating apoptosis, cell survival, differentiation, and the production of inflammation-associated factors (17‑19). It is known that increased ROS production during CP treatment activates several signaling cascades that lead to renal tubular epithelial cell mortality and damage (20‑22).

Apoptosis, a conserved process of programmed cell death in which cells self-destruct, is one of the ROS-activated signaling cascades. ROS

are one of the most crucial apoptosis-inducing stressors (23-26) among a variety of exogenous and endogenous apoptosis-inducing signals.

Senescence is an additional ROS-activated signaling cascade. Cellular senescence is characterized by an unreversible cell cycle arrest that limits the proliferation of dysfunctional cells (27) and is a significant risk factor for the progression of multiple cancers, cardiovascular diseases, and neurodegenerative diseases (28). Recent studies link high levels of ROS production to a faster rate of aging, and low levels of ROS production to extended lifespans (29-31).

Ketone bodies are three biomolecules, including β-hydroxybutyrate (βOHB), acetoacetate, and acetone, that the muscle, brain, heart, and other organs can use as alternative energy sources during prolonged periods of fasting or deprivation (14,32,33). These physiological changes result in a wide range of blood ketones, allowing them to act as metabolic signals to regulate a variety of cellular functions (inhibit lipolysis and oxidative stress, improve neuroprotection, and inhibit histone methylation and acetylation) (34,35). Dietary interventions such as calorie restriction (CR) or ketogenic diet enhance the circulation of βOHB, presumably an anti-aging metabolite that protects against age-related diseases (28,35,36 -38). Multiple published reports have demonstrated that low concentrations of βOHB have anti-inflammatory and anti-oxidant effects (39,40), and exogenous βOHB has demonstrated beneficial therapeutic effects in stressful conditions such as extensive burns (41), hemorrhage shock (42,43), anoxia, hypoxia, and cerebral ischemia (44). In mammals, βOHB decreases the vascular cell senescence and senescence-associated secretory phenotype (SASP), and it has been reported that ketogenic diet significantly increase the lifespan of mice (27,36).

In this study, the protective effects of βOHB against CP-induced injury in human proximal tubule epithelial cells (HK-2) were investigated, with

a focus on the reduction of oxidative stress, apoptosis, and senescence and the increase in proliferation. In addition, the effects of βOHB on oxidative stress-related gene expression and anti-senescence in the CP-induced AKI model were investigated.

2. Materials and Methods

2.1. Cell culture and reagents:

HK-2 cells (an immortalized human proximal tubule epithelial cell line) were purchased from the Korean Cell Line Bank (KCLB) (Seoul, Korea). HK-2 cells were grown in RPMI 1640 medium supplemented with 10% fetal bovine serum (FBS) (Welgene, Gyeonsangbuk-do, Korea) and 1% penicillin/streptomycin antibiotics (Gibco, Grand Island, New York) at 37 ℃ in a 5% CO_2 humidified atmosphere. CP and βOHB were obtained from Sigma-Aldrich (St. Louis, MO, USA).

2.2. Drug treatment:

Different treatment times and conditions apply to each experiment. The details are described in Figure 1. In the first procedure, cells were pre-incubated with βOHB (5 or 10 mM) for 2 hours and then treated with CP (5 or 10 μM) for 24 and 48 hours. In the second procedure, 6 hours after having been treated with CP (5 or 10 μM), the medium was changed to medium containing βOHB (5 or 10 mM) and incubated for 7 days. In the third procedure, after incubation with CP at 5 μM for 24 and 48 hours, the medium was changed to medium containing βOHB (5 or 10 mM), and the optical density (OD) was measured daily. In the fourth procedure, cells were pre-incubated with βOHB (5 or 10 mM) for 2 hours before being treated with CP (5 or 10 μM) for 30 minutes.

2.3. Animals and the CP-induced AKI model:

All the experiments were performed on 7-week-old male C57BL/6J mice that had been purchased from Ja Bio (Gyeonggi-do, Korea). The mice were maintained at a controlled temperature (24 ± 1 ℃), humidity, and lighting (12 : 12 hours light-dark cycle). After one week of acclimatization, the mice were randomly divided into 4 groups: Control, βOHB, CP, and βOHB + CP (n = 7 for each group). Mice in the Control group received a single intraperitoneal (i.p.) injection of normal saline. βOHB were administered into mice in the βOHB group by i.p. injection once a day for 7 days. The CP group mice were administered with CP at 25 mg/kg in a single i.p. injection. To investigate the effects of βOHB on CP-induced AKI, the mice were pre-treated with βOHB per day by i.p. administration once a day for 4 days before and 3 days after CP injection. Blood samples and kidney tissues were collected for further study. The whole experimental procedure is shown in Figure 11A. The Institutional Animal Care and Use Committee (IACUC) of Keimyung University, School of Medicine approved this study (KM-2020-16R1).

2.4. Cell viability and morphology:

To determine cell viability and morphology, cells were seeded into 96-well plates (1×10^4 cells per well). Cells were treated according to treatment procedure 1 (Figure 1). Cell viability was measured using Cell Counting Kit-8 (CCK-8) (Dojindo, Kumamoto, Japan) according to the manufacturer's instructions. The CCK-8 reagent was briefly added to each well, followed by incubation for 1 hour at 37 ℃ in a 5% CO_2 humidified atmosphere. Absorbance was measured at 450 nm using a microplate reader (Infinite M200 Pro, Tecan, Mannedorf, Switzerland).

Cell viability was expressed as a percentage of the control. Changes in cell morphology caused by CP and βOHB alone or in combination were analyzed by microscopy. Cells were viewed and captured using an inverted microscopy (DMi1, Leica, Wetzlar, Germany) under phase-contrast illumination.

2.5. Cell cytotoxicity:

To determine cytotoxicity, cells were seeded into 96-well plates (1 × 10^4 cells per well). Cells were treated according to drug treatment procedure 1 (Figure 1). Cell cytotoxicity was determined by measuring lactate dehydrogenase (LDH) released from HK-2 cells using a Cytotoxicity LDH Assay Kit-WST (Dojindo, Kumamoto, Japan) according to the manufacturer's instructions. In brief, 100 μL of Working Solution was added to the wells and then cells were incubated for a further 30 minutes at 37 ℃ until 50 μL of Stop Solution was added. Absorbance was measured at 490 nm using a microplate reader (Infinite M200 Pro, Tecan, Mannedorf, Switzerland). The relative activity of LDH (%) was calculated as [Cytotoxicity (%) = (Test Substance - Low Control / High Control - Low Control) × 100].

2.6. Western blot analysis:

Cells were seeded into 60-mm dishes (3 × 10^5 cells) for western blot analysis. Cells were treated according to drug treatment procedure 1 (Figure 1). Harvested cells were lysed in radioimmunoprecipitation assay (RIPA) buffer (Thermo Scientific, Boston, MA, USA) containing 0.2 M phenylmethylsulfonyl fluoride (PMSF) (Cell Signaling Technology,

Beverly, MA, USA) and protease inhibitors (PI) (Gendepot, Katy, TX, USA). Lysates were centrifuged at 7,500 g for 20 minutes at 4 ℃ and the supernatant was collected. The lysates were quantified using the bicinchoninic acid (BCA) Protein Assay Kit (Thermo Scientific, Boston, MA, USA). Thirty μg of protein was separated by sodium dodecyl sulfate polyacrylamide gel electrophoresis (SDS-PAGE). The protein was transferred to a nitrocellulose membrane (GE Healthcare, Little Chalfont, UK). The membranes were blocked in 5% skim milk in tris buffered saline with Tween 20 (TBS-T) (50 mmol/L NaCl, 10 mmol/L Tris-HCl, and 0.25% Tween-20) for 30 minutes at room temperature. Membranes were incubated with anti-cleaved caspase-3, anti-cleaved PARP, anti-ɣ H2AX, anti-TNF-α, anti-MMP3 (1:1,000 dilution, Cell Signaling Technology, Beverly, MA, USA), and anti-p16 (1:1,000 dilution, Thermo Scientific, Boston, MA, USA) primary antibodies at 4 ℃ overnight. Beta-actin (1:2,000 dilution, Sigma-Aldrich, St. Louis, MO, USA) was used as an internal control. The membranes were washed three times with TBS-T for 10 minutes each and incubated with horseradish peroxidase (HRP)-conjugated secondary antibodies (1:3,000 dilution, Cell Signaling Technology, Beverly, MA, USA) for 2 hours at room temperature. Protein bands were detected using Lumi-Pico solution (Dogen, Seoul, Korea). LAS-3000 was used to detect protein-specific signals (Fujifilm, Tokyo, Japan).

2.7. Real-time reverse transcription-polymerase chain reaction (RT-PCR) analysis:

Cells were seeded into 6-well plates (1.5 × 10^5 cells per well) for real-time PCR. Cells were treated according to drug treatment procedure

1 (Figure 1). Total RNA was extracted from cultured HK-2 cells or kidney tissues using Trizol reagent (Invitrogen, Carlsbad, CA, USA) according to the manufacturer's protocol. A NanoDrop 2000 spectrophotometer (NonoDrop Technologies, Wilmington, DE, USA) was used to measure RNA purity and concentration. Complementary DNA (cDNA) was synthesized from 4 μg of RNA using Moloney Murine Leukemia Virus (M-MLV) reverse transcriptase (Promega, Madison, WI, USA). SYBR Green PCR Master Mix (Toyobo, Osaka, Japan) was used for real-time PCR. The real-time PCR was performed using 10 μL of SYBR Green PCR Master Mix, 0.5 μL of forward and reverse primers at 10 pmole/μL, 7 μL of water, and 2 μL of template cDNA for a total volume of 20 μL. Real-time PCR used the following parameters: initial denaturation at 95 ℃ for 30 seconds, amplification at 45 cycles performed at 95 ℃ for 5 seconds, 60 ℃ for 10 seconds, and 72 ℃ for 15 seconds, melting curve at 95 ℃ for 10 seconds, 65 ℃ for 1 minute, cooling at 37 ℃ for 10 minutes with gene-specific primers (Table 1). Quantification by real-time PCR was used with a LightCycler 480 (Roche, Basel, Switzerland). The comparative Ct ($2^{-\Delta\Delta Ct}$) method was used to quantify mRNA levels, which were normalized to the levels of the respective housekeeping genes, *β-actin*. Primer sequences (Macrogen, Seoul, Korea) are shown in Table 1.

2.8. Senescence-associated β-galactosidase (SA-β-gal) staining assay:

For the SA-β-gal staining assay, cells were seeded into 6-well plates (1.5 × 10^5 cells per well). Cells were treated according to drug treatment procedure 1 (Figure 1). SA-β-gal staining was performed according to

Dimri et al. (45). Briefly, cells were washed twice with phosphate-buffered saline (PBS) and fixed with 4% paraformaldehyde (PFA) (Fujifilm Wako, Osaka, Japan) for 10 minutes at room temperature. The cells were washed twice with PBS, cleared completely, and then incubated overnight in a solution of fresh X-gal staining [1 mg/ml 5-bromo-4-chloro-3-indolyl-β-D-galactopyranoside (X-Gal), 5 mM potassium ferricyanide trihydrate, 5 mM potassium ferricyanide crystalline, and 2 mM magnesium chloride in PBS, pH 6.0] at 37 ℃ without CO_2. The cells were then visualized under a microscopy (CKX53, Olympus, Tokyo, Japan) to quantify the percentage of positive SA-β-gal staining cells.

Quantitative analysis of cultured cells was performed with the Cellular Senescence Plate Assay Kit SPiDER-βGal (Dojindo, Kumamoto, Japan) in accordance with the manufacturer's protocol. Cells were seeded into 96-well plates ($1 × 10^4$ cells per well). Cells were treated according to drug treatment procedure 1 (Figure 1). In brief, cells were lysed with Lysis Buffer for 10 minutes at room temperature, followed by incubation with SPiDER-βGal Working Solution for 30 minutes in a 37 ℃ in a 5% CO_2 humidified atmosphere. The excitation wavelength of 535 nm and the emission wavelength of 580 nm were then measured using a microplate reader (Infinite M200 Pro, Tecan, Mannedorf, Switzerland) after the addition of the Stop Solution. The Cell Count Normalization Kit (Dojindo, Kumamoto, Japan) was used to adjust the number of cells between wells.

For SA-β-gal staining, kidney tissues were embedded in paraffin. Paraffin tissues were sectioned at 4 μm thickness using a Microtome (HM 325 Rotary Microtome, Thermo Scientific, Boston, MA, USA). Tissues were rehydrated with xylene and a series of graded ethanols and incubated in a fresh X-gal staining solution (pH 4.0) for 16 hours

at 37 ℃ without CO_2. All histological assessments were performed by microscopic examination of stained sections (DM750, Leica, Wetzlar, Germany).

2.9. Colony formation assay:

For the colony formation assay, HK-2 cells were seeded into 6-well plates (1×10^3 cells per well). Cells were treated according to drug treatment procedure 2 (Figure 1). After 6 hours of incubation with CP, the cells were grown in βOHB in the culture medium for 1 week. Cells were fixed with methanol for 15 minutes and stained with 0.5% crystal violet (Sigma-Aldrich, St. Louis, MO, USA) in 25% methanol for 1 hour at room temperature. After being rinsed with distilled water, colonies were counted for each sample and images of the stained colonies were visualized under a microscopy (CKX53, Olympus, Tokyo, Japan), and colonies were calculated using Image J software (National Institutes of Health, Bethesda, MD, USA). For quantitative analysis, the colonies were resuspended in 10% acetic acid for 1 hour at room temperature by shaking. The absorbance of the crystal violet was measured at 590 nm using a microplate reader (Infinite M200 Pro, Tecan, Mannedorf, Switzerland).

2.10. Cell proliferation and growth curve:

HK-2 cells proliferation was measured by CCK-8 (Dojindo, Kumamoto, Japan). Cells were seeded into 96-well plates (0.8×10^4 cells per well). Cells were treated according to drug treatment procedure 3 (Figure 1). All experiments were performed in triplicate. At 1, 2, and 3

days after incubation, CCK-8 reagent was added to each well, incubated for 1 hour at 37 ℃ in a 5% CO_2 humidified atmosphere, and the results were analyzed by a plate reader at 450 nm using a microplate reader (Infinite M200 Pro, Tecan, Mannedorf, Switzerland).

2.11. ROS measurement assay:

ROS was assessed using 2',7'-dichlorofluorescein diacetate (DCFDA) (Sigma-Aldrich, St. Louis, MO, USA), which enters the cell and reacts with reactive oxygen to produce a green fluorescent dye. HK-2 cells were seeded into 12-well plates (7×10^4 cells per well). Cells were treated according to drug treatment procedure 4 (Figure 1). After treatment, cells were washed with Hanks balanced salt solution (HBSS) (Gibco, Grand Island, New York) and incubated with 30 μM (working solution) DCFDA for 30 minutes at 37 ℃ in a 5% CO_2 humidified atmosphere. Cells were washed twice with HBSS and observed under fluorescence microscopy (CKX53, Olympus, Tokyo, Japan). DCFDA green fluorescence per cell was quantified using Image J software (National Institutes of Health, Bethesda, MD, USA).

2.12. Assessment of renal function:

Blood samples were collected in tubes and centrifuged at 2,000 g for 20 minutes to isolate the serum. SCr and BUN (Abcam, Cambridge, UK) levels were measured according to the manufacturer's protocol. Absorbance was measured using a microplate reader at a wavelength of 570 nm. Serum levels of kidney injury molecular 1 (KIM1) were measured using an enzyme-linked immunosorbent assay (ELISA) kit

(Abcam, Cambridge, UK) according to the manufacturer's protocol. A microplate reader was used to measure OD at 450 nm (Infinite M200 Pro, Tecan, Mannedorf, Switzerland), and the concentration of KIM1 in each sample was calculated from the standard curve.

2.13. Histologic analysis of the kidney:

Kidney tissues were fixed in 10% formalin, embedded in paraffin, and cut into 4 μm thick sections using a Microtome (HM 325 Rotary Microtome, Thermo Scientific, Boston, MA, USA). Tissues were rehydrated through xylene and a graded series of ethanol. Hematoxylin and eosin (H&E) and periodic acid-Schiff (PAS) staining kits (Scytek Laboratories, Inc., Logan, UT, USA) were used. Staining was performed according to the manufacturer's instructions. Stained sections were examined under light microscopy (DM750, Leica, Wetzlar, Germany).

2.14. ROS measurement in the kidney:

Superoxide levels in kidney tissue were measured by staining the freshly prepared paraffin sections with dihydroethidium (DHE) (Sigma-Aldrich, St. Louis, MO, USA). Sections were cut into 4 μm thick slices and deparaffinized in 3 xylene for 5 minutes each. Sections were rehydrated in graded alcohols, and 3 times washed in PBS. Sections were incubated with 10 μM DHE for 30 minutes in a humidified and dark chamber at room temperature and then counterstained with 4′,6-diamidino-2-pheylindole (DAPI) (Sigma-Aldrich, St. Louis, MO, USA). Mounting was performed using ProLong Gold Antifade Mountant (Invitrogen, Gaithersburg, MD, USA), fluorescence

images were acquired using a fluorescence microscopy (Axio Observer A1, Carl Zeiss, Jena, Germany), and Image J (National Institutes of Health, Bethesda, MD, USA) was used to quantify DHE-positive cellular structures.

2.15. Immunohistochemistry (IHC) analysis:

Kidney tissue sections were deparaffinized through 3 xylene washes of 5 minutes each, after drying at 60 ℃ for 30 minutes. The sections were rehydrated in graded alcohols and then incubated in 30% hydrogen peroxide for 15 minutes. For antigen retrieval, sections were incubated in 10 mM citrate buffer (pH 6.0) at 95 ℃. Sections were incubated with an 8-hydroxy-2′-deoxyguanosine (8-OHdG) antibody (1:100 dilution, Santa Cruz Biotechnology, Dallas, TX, USA) at 4 ℃ overnight. After washing with PBS, the sections were incubated with secondary antibody (1:200 dilution, Abcam, Cambridge, UK) for 1 hour at room temperature. The immunoreaction sections were visualized with 3,3'-diaminobenzidine (DAB) substrate kit (Vector Laboratories, Burlingame, CA, USA) (brown color indicates 8-OHdG protein) and counterstained with hematoxylin (Dako, Glostrup, Denmark). Stained sections were examined by light microscopy (DM750, Leica, Wetzlar, Germany). A light microscope equipped with an imaging system was used to quantify the stained areas. Quantitative analysis of the 8-OHdG areas (with brown staining) was performed using Image J (National Institutes of Health, Bethesda, MD, USA).

2.16. Statistical analysis:

All experiments consisted of a minimum of three independent experiments. Results are presented as the mean ± standard deviation (SD) (n $\geq$ 3). Student's t-test was used for statistical analysis, p value of $<$ 0.05 was considered to indicate statistical significance.

Table. Details of Primer Pair Sequences

Species	Name	Sequences of primers	
Human	*β-actin*	Forward : 5' – GGACTTCGAGCAAGAGATGG – 3'	
		Reverse : 5' – AGCACTGTGTTGGCGTACAG – 3'	
	Bcl-2	Forward : 5' – GTCTGGGAATCGATCTGGAA – 3'	
		Reverse : 5' – AATGCATAAGGCAACGATCC – 3'	
	Bax	Forward : 5' – ATGTTTTCTGACGGCAACTTC – 3'	
		Reverse : 5' – AGTCCAATGTCCAGCCCAT – 3'	
	γ-H2AX	Forward : 5' – CAACAAGAAGACGCGAATCA – 3'	
		Reverse : 5' – CGGGCCCTCTTAGTACTCCT – 3'	
	p16 (CDKN2A)	Forward : 5' – ATATGCCTTCCCCCACTACC – 3'	
		Reverse : 5' – CCCCTGAGCTTCCCTAGTTC – 3'	
	p21 (CDKN1A)	Forward : 5' – ATGAAATTCACCCCCTTTCC – 3'	
		Reverse : 5' – CCCTAGGCTGTGCTCACTTC – 3'	
	p27 (CDKN1B)	Forward : 5' – TCAAACGTGCGAGTGTCTAA – 3'	
		Reverse : 5' – CCATGTCTCTGCAGTGCTTC – 3'	
	TNF-a	Forward : 5' – TCCTTCAGACACCCTCAACC – 3'	
		Reverse : 5' – AGGCCCCAGTTTGAATTCTT – 3'	

Table. Details of Primer Pair Sequences (continued)

Species	Name	Sequences of primers	
Human	*MMP3*	Forward : 5' – GCAGTTTGCTCAGCCTATCC – 3'	
		Reverse : 5' – GAGTGTCGGAGTCCAGCTTC – 3'	
	CAT	Forward : 5' – AGCGTTCATCCGTGTAACCC – 3'	
		Reverse : 5' – AATAATCCAATCATCCGTCA – 3'	
	SOD1	Forward : 5' – AGGGCATCATCAATTTCGAG – 3'	
		Reverse : 5' – ACATTGCCCAAGTCTCCAAC – 3'	
	GPX1	Forward : 5' – GCAGTGCTGCTGTCTCGGGG – 3'	
		Reverse : 5' – CTGACACCCGGCACTTTATT – 3'	
	GSR	Forward : 5' – TCAGCTCACCACAACCTCTG – 3'	
		Reverse : 5' – GAGACCAGCCTGACCAACAT – 3'	
Mouse	*β-actin*	Forward : 5' – AGCCATGTACGTAGCCATCC – 3'	
		Reverse : 5' – TTTCCCTCTCAGCTGTGGTG – 3'	
	KIM1	Forward : 5' – GCTCAGGGTCTCCTTCACAG – 3'	
		Reverse : 5' – CAACATGTCGTTGTGATTCC – 3'	
	γ-H2AX	Forward : 5' – GGTCAGAGAGACGCTTACCG – 3'	
		Reverse : 5' – GCCCATTAAATCTCCCCACT – 3'	

Table. Details of Primer Pair Sequences (continued)

Species	Name	Sequences of primers
Mouse	*p16 (CDKN2A)*	Forward : 5' – CTTCTGCTCAACTACGGTGC – 3' Reverse : 5' – GCACGATGTCTTGATGTCCC – 3'
	p21 (CDKN1A)	Forward : 5' – AGCCCTCACTCTGTGTGTCT – 3' Reverse : 5' – CACTAAGGGCCCTACCGTCC – 3'
	IL-6	Forward : 5' – CCTTCTTGGGACTGATGCTG – 3' Reverse : 5' – TCATTTCCACGATTTCCCAG – 3'
	IL-1a	Forward : 5' – CCTTATTTCGGGAGTCTATT – 3' Reverse : 5' – ATAGTATCATATGTCGGGGT – 3'
	IL-1β	Forward : 5' – GCCCATCCTCTGTGACTCAT – 3' Reverse : 5' – AGGCCACAGGTATTTTGTCG – 3'
	CAT	Forward : 5' – GTCTGGGACTTCTGGAGTCT – 3' Reverse : 5' – CAAGTTTTTGATGCCCTGGT – 3'
	SOD1	Forward : 5' – CCAGTGCAGGACCTCATTTT – 3' Reverse : 5' – TTGTTTCTCATGGACCACCA – 3'
	GPX1	Forward : 5' – CCGTGTATGCCTTCTCCGCG – 3' Reverse : 5' – ACGCTTCTGCAGATCGTTCA – 3'

Table. Details of Primer Pair Sequences (continued)

Species	Name	Sequences of primers
Mouse	*GSR*	Forward : 5' - CACGACCATGATTCCAGATG - 3' Reverse : 5' - CAGCATAGACGCCTTTGACA - 3'

Bax: bcl-2 associated X; *Bcl-2:* B-cell lymphoma 2; *CAT:* catalase; *GPX1:* glutathione peroxidase 1; *GSR:* glutathione reductase; *IL-1α:* interleukin-1 alpha; *IL-1β:* interleukin-1 beta; *IL-6:* interleukin 6; *KIM1:* kidney injury molecule 1; *MMP3:* matrix metallopeptidase 3; *p16:* cyclin-dependent kinase inhibitor 2A; *p21:* cyclin-dependent kinase inhibitor 1A; *p27:* cyclin-dependent kinase inhibitor 1B; *SOD1:* superoxide dismutase 1; *TNF-α:* tumor necrosis factor alpha; ɣ*H2AX:* gamma-H2A.X variant histone.

3. Results

3.1. Protective effect of βOHB on CP-induced cytotoxicity in HK-2 cells:

To determine whether βOHB protects HK-2 cells from CP-induced cytotoxicity, HK-2 cells were pre-treated with 5 or 10 mM of βOHB for 2 hours, then treated with 5 or 10 μM of CP for 24 or 48 hours. Light microscopy images of living HK-2 cells revealed morphological growth (Figure 2A&B). Using the CCK-8 assay, the cell viability of βOHB and CP treated HK-2 cells was determined. The cell viability assay revealed that treatment with 5 or 10 μM CP for 24 hours resulted in 60% cell viability relative to the control, whereas treatment with 5 or 10 μM CP for 48 hours resulted in 40% cell viability relative to the control and 30% cell viability relative to the control. Quantitatively, the cell viability of cells treated with CP + βOHB was greater than that of cells treated with CP alone (Figure 3A). In addition, LDH cell cytotoxicity assay revealed that treatment with 5 or 10 μM of CP for 24 or 48 hours increased cell cytotoxicity relative to the control, whereas cells treated with CP + βOHB decreased cell cytotoxicity relative to CP alone (Figure 3B). Real-time PCR and western blot analysis using apoptosis markers were used to further validate these results. Figure 4A demonstrates that treatment with CP alone increased the cleavage of caspase-3 and PARP, whereas treatment with CP + βOHB decreased the cleavage of caspase-3 and PARP. Moreover, *Bax* expression, an indicator of the level of pro-apoptosis, revealed an increase in cells treated with 5 or 10 μM of CP for 24 or 48 hours compared to the

control and a decrease in cells treated with CP + βOHB compared to CP alone (Figure 4B). Figure 4C demonstrates that *Bcl-2* expression, an indicator of anti-apoptosis levels, shows the opposite effect of *Bax*.

3.2. Protective effect of βOHB on CP-induced senescence in HK-2 cells:

Analysis of SA-β-gal staining as a senescent cell marker was performed. The HK-2 cells were pre-treated with 5 or 10 mM of βOHB for 2 hours, then treated with 5 or 10 μM of CP for 24 or 48 hours. The SA-β-gal staining assay revealed that the number of positively stained cells was considerably low in the CP + βOHB than that in the CP alone (Figure 5A). To quantify this staining, the number of SA-β-gal positive (blue) cells relative to the total number of cells was manually determined in at least five images per condition (Figure 5B). In addition, the SPiDER-βGal assay was used to measure the activity of SA-β-gal. The SPiDER-βGal assay revealed that treatment with 5 or 10 μM of CP for 24 or 48 hours resulted in an increase relative to the control, whereas cells treated with CP + βOHB exhibited a decrease relative to CP alone (Figure 5C). In addition, senescence markers including ɣ-H2AX, p16, TNF-α, and MMP3 were analyzed using western blotting. Figure 6A demonstrates that treatment with CP alone upregulates senescence markers, whereas treatment with CP + βOHB downregulates senescence markers. Additionally, real-time PCR was utilized to identify senescence markers. Figure 6B demonstrates that treatment with CP alone upregulates senescence markers, whereas treatment with CP + βOHB downregulates senescence markers.

3.3. Effect of βOHB on CP-induced colony formation and cell proliferation in HK-2 cells:

To determine whether βOHB regulates CP-induced colony formation, HK-2 cells were treated with 5 or 10 mM of βOHB for 7 days after being stimulated with 5 or 10 μM of CP for 6 hours. Colony formation assay was conducted to confirm cell proliferation. CP at 5 μM resulted in 10% colony formation and CP at 10 μM resulted in 1% colony formation. Colony formation of βOHB alone did not differ from that of the control. In addition, treatment with CP + βOHB enhanced colony formation proportionally to the βOHB concentration (Figure 7A&B). To determine whether βOHB regulates CP-induced cell proliferation, HK-2 cells were induced with 5 μM of CP for 24 or 48 hours, followed by 3 days of treatment with 5 or 10 mM of βOHB, and CCK-8 assay was performed. Figure 8 demonstrates that the CP + βOHB treatment results in greater growth than the CP treatment.

3.4. Preventive effect of βOHB on CP-induced intracellular ROS accumulation in HK-2 cells:

One of the many pathways implicated in CP-induced nephrotoxicity is oxidative stress. To determine whether βOHB has antioxidant properties against CP-induced oxidative stress, HK-2 cells were pre-treated with βOHB for 2 hours, then exposed to 5 or 10 μM of CP for 30 minutes, and then stained with membrane-permeable ROS indicator DCFDA. The representative fluorescence images demonstrate that CP significantly increases DCFDA-positive cells, whereas βOHB prevented this effect (Figure 9A). Analyses of quantitative data demonstrates that treatment

with 5 or 10 mM of βOHB significantly decreases the fluorescence intensity of DCFDA by CP (Figure 9B). In addition, real-time PCR was used to analyze ROS scavenger markers such as *CAT, SOD1, GPX1, and GSR.* Figure 10 demonstrates that treatment with CP alone downregulates ROS scavenger markers, whereas treatment with CP + β OHB upregulates these markers.

3.5. Effects of βOHB on kidney damage in CP-induced AKI mice:

The experimental design for the investigation into the protective effect of βOHB against CP-induced AKI in C57BL/6 mice is shown in Figure 11A. On the 3 days following CP treatment, kidney injury was visible in the CP-treated group, but pre-treatment with βOHB prevented it (Figure 11B). H&E and PAS staining confirmed the morphological alterations in the kidneys. Histological staining revealed tubular damage and interstitial fibrosis in the kidneys of the CP-treated groups, which were significantly reduced in βOHB-pretreated groups (Figure 11C). In addition, real-time PCR and ELISA demonstrate a significant decrease in KIM1 in the βOHB-pretreated group. BUN and SCr, which are markers of renal function, were also validated by ELISA in serum. The CP-treated group showed higher levels of KIM1, BUN, and SCr than the Control or βOHB-only groups. However, CP-pretreated with βOHB group showed significantly decreased KIM1, BUN, and SCr levels relative to the CP-treated group (Figure 12A‐D).

3.6. Anti-senescence effect of βOHB on CP-induced AKI mice:

To determine whether CP-induced tubular injury is associated with cellular senescence, SA-β-gal staining in the kidneys of mice with CP-induced AKI was examined. The SA-β-gal positive area (blue) was significantly increased in the CP-treated group and inhibited by βOHB (Figure 13A&B). In addition, real-time PCR demonstrates upregulation of senescence markers and SASP genes in the kidneys of CP-induced AKI mice and confirms that βOHB inhibits the expression of senescence (Figure 14A) and SASP genes (Figure 14B).

3.7. Effect of βOHB on ROS production in CP-induced AKI mice:

DHE staining was used to assess ROS production in mice kidneys. DHE staining demonstrates a substantial increase in ROS production in the CP-treated group, which was reduced by βOHB pre-treatment (Figure 15A&B). In addition, oxidative stress biomarkers, such as 8-OHdG, were determined using IHC staining. The 8-OHdG staining increased significantly in the CP-treated group, similar to the DHE staining, and was reduced by βOHB pre-treatment (Figure 15C&D). Real-time PCR was also used to determine the expression of ROS scavenger markers *CAT, SOD1, GPX1,* and *GSR* in the kidneys of mice with CP-induced AKI. Figure 16 demonstrates that the CP-treated group downregulates ROS scavenger markers, whereas the βOHB-pretreated group upregulates ROS scavenger markers.

In conclusion, CP-induced kidney injury induces ROS, which increase apoptosis and senescence and decrease proliferation, leading to the development of AKI. However, βOHB prevents the induction of ROS and thus protects against the development of AKI (Figure 17).
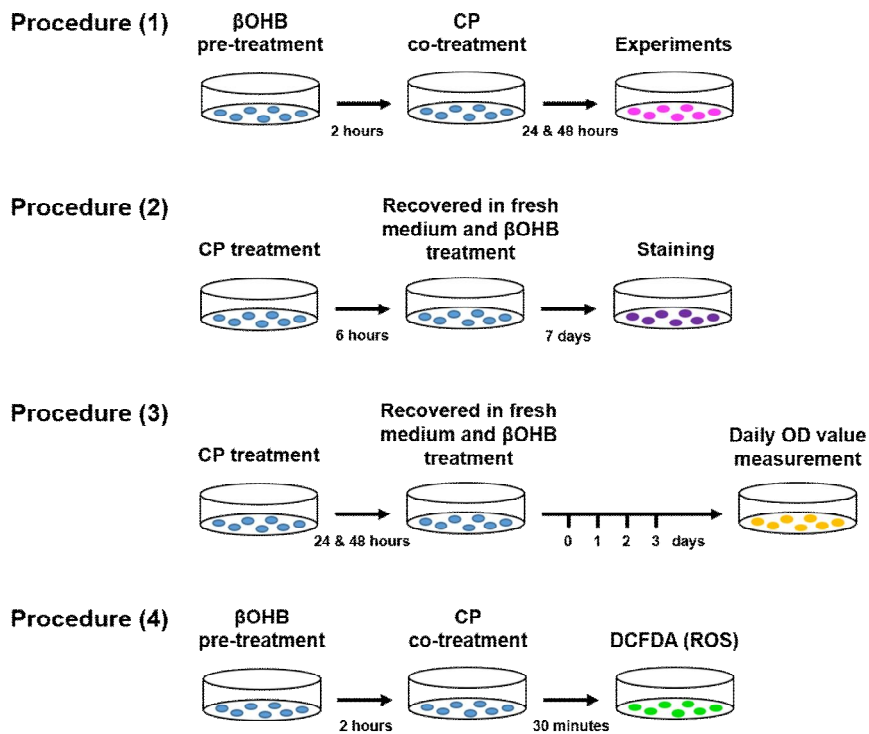
Figure 1. Schematic showing the course of the different experimental conditions. Illustration of the experimentally determined treatment conditions for HK-2 cells. Procedure 1 was carried out to determine apoptosis and senescence. Procedure 2 was an executed to examine the colony formation. Procedure 3 was performed for a growth curve analysis. Procedure 4 was done to investigate ROS productions. CP: cisplatin; DCFDA: 2',7'-dichlorofluorescein diacetate; OD: optical density; ROS: reactive oxygen species; βOHB: β-hydroxybutyrate.

A βOHB (mM)   0   5   10

CP 0 μM

CP 5 μM

CP 10 μM

Scale bar : 250 μm

B βOHB (mM)   0   5   10

CP 0 μM

CP 5 μM

CP 10 μM
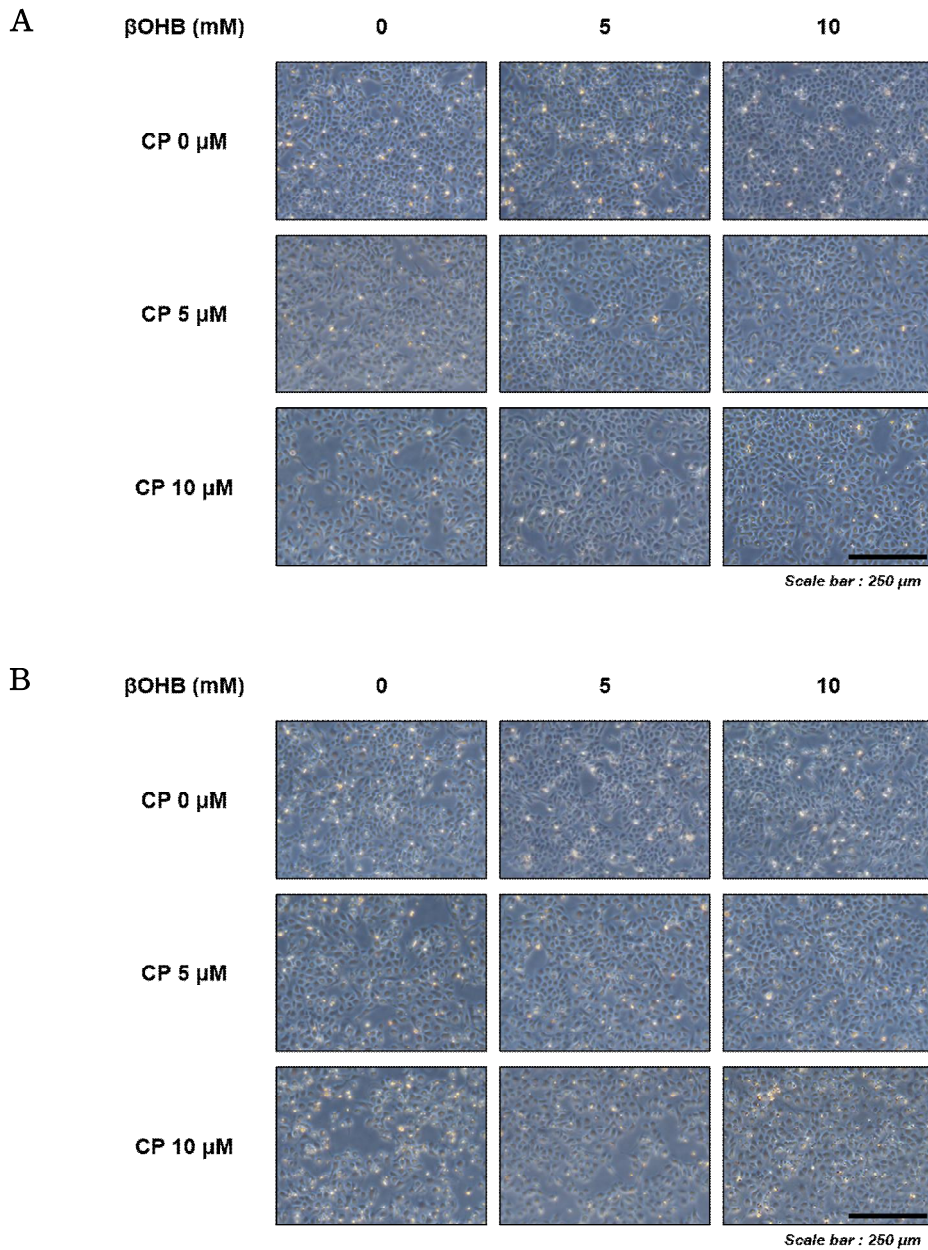
Scale bar : 250 μm

Figure 2. Morphological changes of HK-2 cells. Cell morphological changes were observed by light microscopy (original magnification × 10; scale bar = 250 μm). HK-2 cells were pre-incubated with different concentrations of βOHB (5 or 10

mM) for 2 hours before treatment with different concentrations of CP (5 or 10 μM) for 24 and 48 hours. **(A)** 24 hours treatment, **(B)** 48 hours treatment. CP: cisplatin; β OHB: β-hydroxybutyrate.

A

24 hours

48 hours
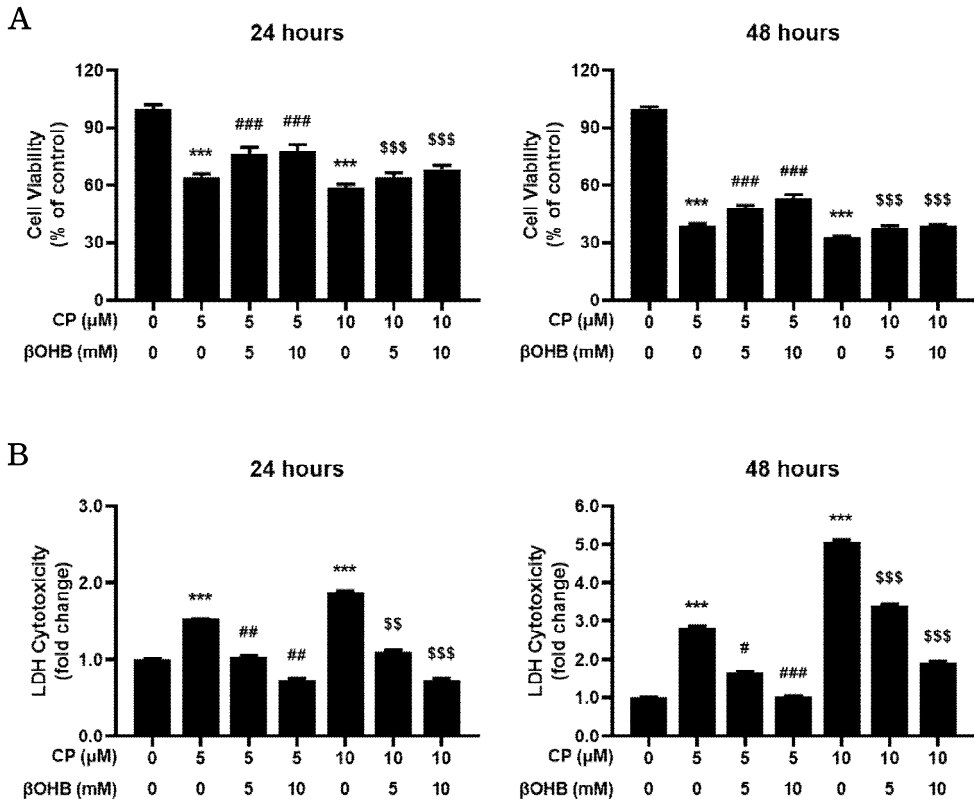

B

24 hours

48 hours

Figure 3. Effects of βOHB on cytotoxicity in CP-treated HK-2 cells. HK-2 cells were pre-incubated with different concentrations of βOHB (5 or 10 mM) for 2 hours before treatment with different concentrations of CP (5 or 10 μM) for 24 and 48 hours. **(A)** Cell viability was evaluated via the CCK-8 assay. **(B)** Cell cytotoxicity was evaluated via the LDH assay. The left panel is a 24 hours treatment, and the right panel is a 48 hours treatment. Data are the mean ± SD. Experiments were performed at least three times independently. Significant differences are indicated: $***$ $p < 0.001$ versus control; # $p < 0.05$, ## $p < 0.01$, ### $p < 0.001$ versus CP 5 μM; \$\$ $p < 0.01$, \$\$\$ $p < 0.001$ versus CP 10

μM. CCK-8: Cell Counting Kit-8; CP: cisplatin; LDH: lactate dehydrogenase; βOHB: β-hydroxybutyrate.
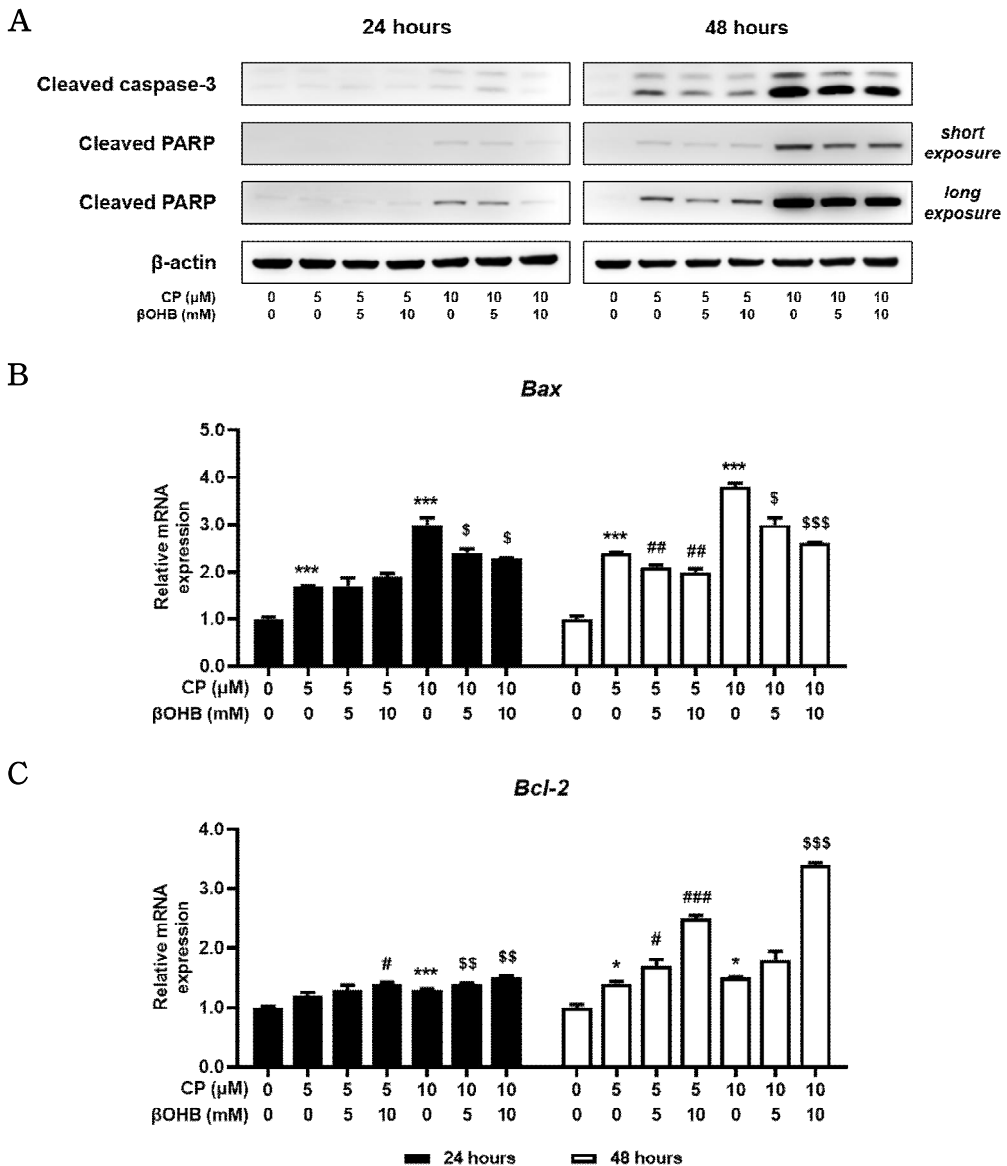
A

B

Bax

C

Bcl-2

■ 24 hours   □ 48 hours

Figure 4. Analysis of apoptosis gene expression with βOHB in CP-treated HK-2 cells. HK-2 cells were pre-incubated with different concentrations of βOHB (5 or 10 mM) for 2 hours before treatment with different concentrations of CP (5 or 10 μM) for 24 and 48 hours. (A) Western blot analysis of

apoptotic markers (cleaved caspase-3, cleaved PARP) in HK-2 cells. **(B & C)** Real-time PCR analysis performed in HK-2 cells. The pro-apoptotic marker *Bax* **(B)** and the anti-apoptotic marker *Bcl-2* **(C)** were determined. Data are the mean ± SD. Experiments were performed at least three times independently. Significant differences are indicated: ∗ $p < 0.05$, ∗∗∗ $p < 0.001$ versus control; # $p < 0.05$, ## $p < 0.01$, ### $p < 0.001$ versus CP 5 μM; $ $p < 0.05$, $$ $p < 0.01$, $$$ $p < 0.001$ versus CP 10 μM. *Bax: B*cl-2 associated X; *Bcl-2:* B-cell lymphoma 2; CP: cisplatin; βOHB: β-hydroxybutyrate.
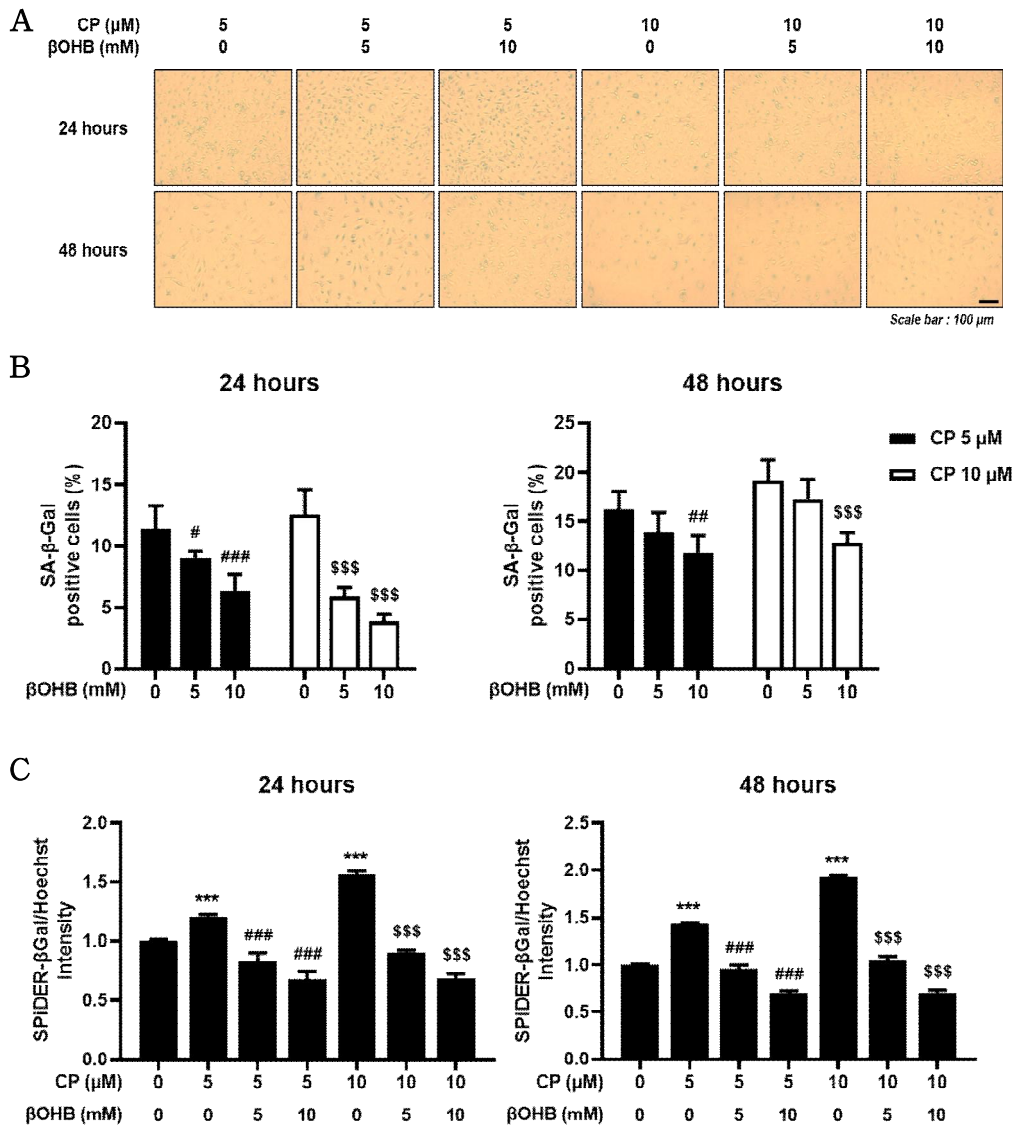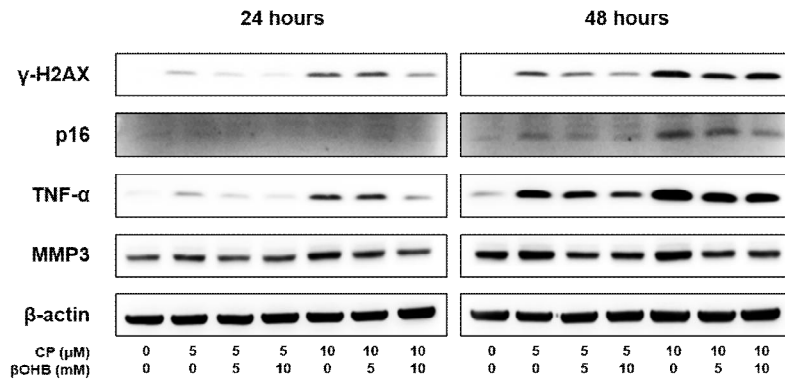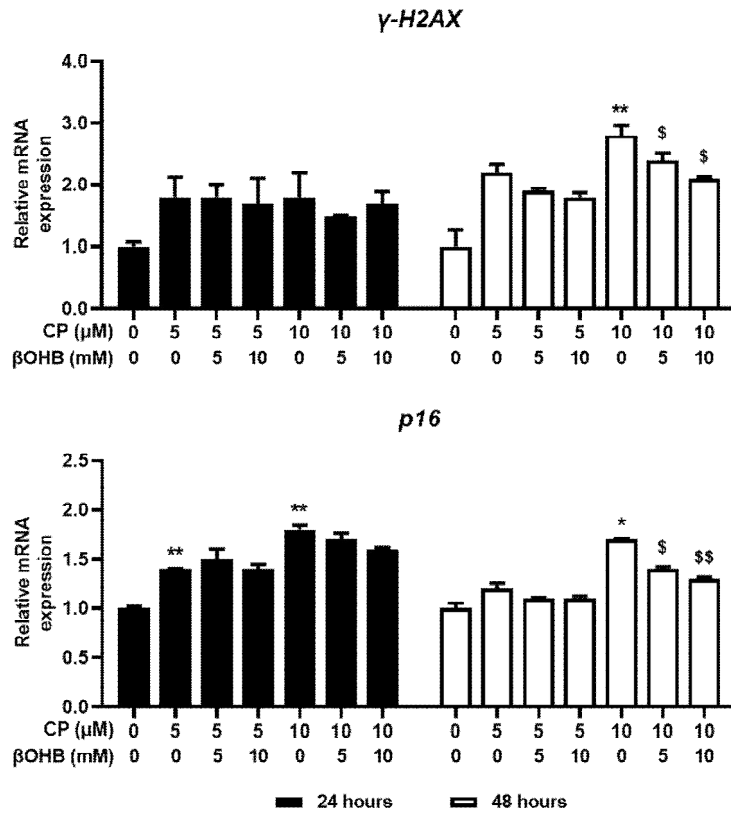
Figure 5. Effect of βOHB on anti-senescence in CP-treated HK-2 cells. HK-2 cells were pre-incubated with different concentrations of βOHB (5 or 10 mM) for 2 hours before treatment with different concentrations of CP (5 or 10 μM) for 24 and 48 hours. (A) Representative microscopy of the staining of SA-β-gal in HK-2 cells (original magnification ×

20; scale bar = 100 μm). (**B**) The number of SA-β-gal positive cells (blue) was used to quantify cellular senescence. (**C**) SA-β-gal activities were measured on HK-2 cells using a SPiDER-βGal Cellular Senescence Plate Assay Kit. Cell counts between wells were adjusted using the Cell Count Normalization Kit. Data are the mean ± SD. Experiments were performed at least three times independently. Significant differences are indicated: ∗∗∗ $p < 0.001$ versus control; # $p < 0.05$, ## $p < 0.01$, ### $p < 0.001$ versus CP 5 μM; $$$ $p < 0.001$ versus CP 10 μM. CP: cisplatin; SA-β-gal: senescence-associated β-galactosidase; βOHB: β-hydroxybutyrate.

A

| | 24 hours | | | | | | | 48 hours | | | | | | |

B

γ-*H2AX*

p16

■ 24 hours   □ 48 hours

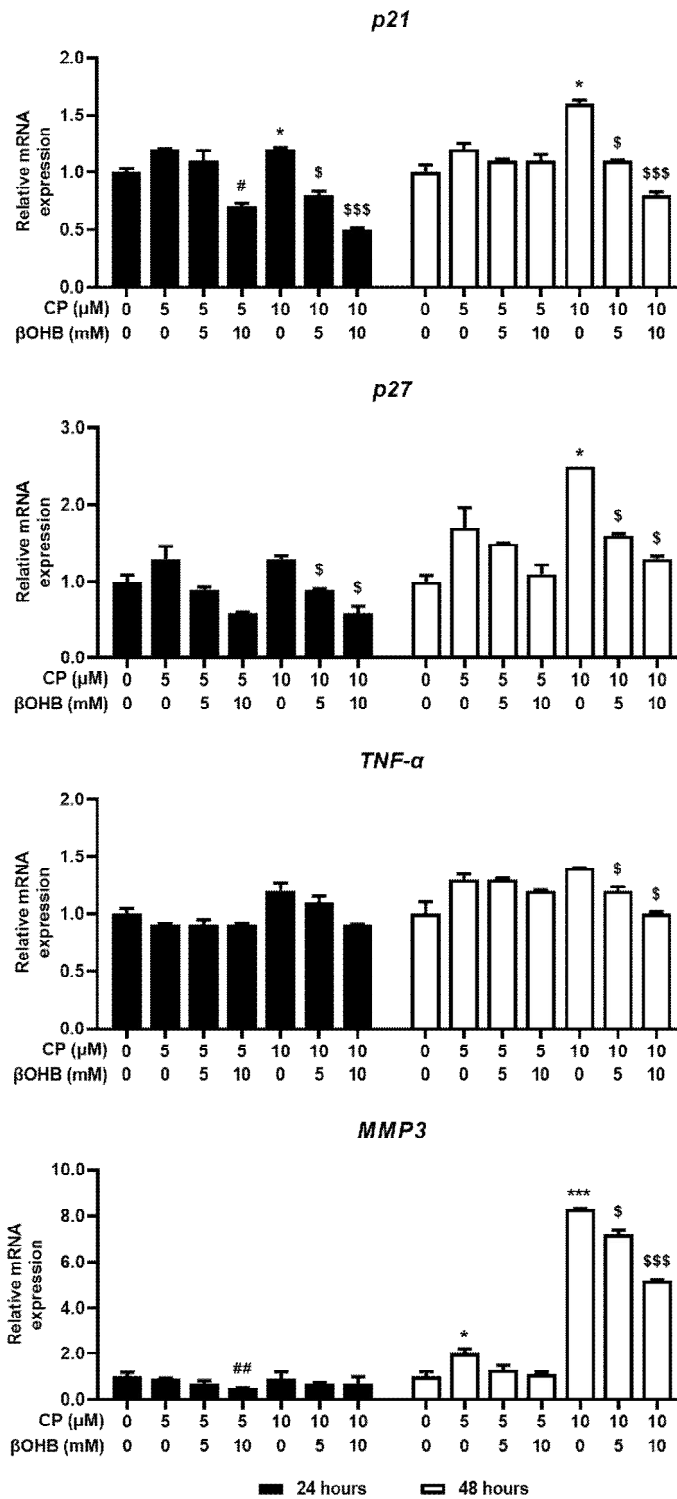(continued)

B

p21

p27

TNF-α

MMP3

Figure 6. Analysis of senescence gene expression with βOHB in CP-treated HK-2 cells. HK-2 cells were pre-incubated with different concentrations of βOHB (5 or 10 mM) for 2 hours before treatment with different concentrations of CP (5 or 10 μM) for 24 and 48 hours. (A) Western blot analysis of senescence markers (ɣ-H2AX, p16, TNF-α, and MMP3) expression in HK-2 cells. (B) Real-time PCR analysis of senescence genes (*ɣ-H2AX, p16, p21, p27, TNF-α, and MMP3*) in HK-2 cells. Data are the mean ± SD. Experiments were performed at least three times independently. Significant differences are indicated: $*$ $p < 0.05$, $**$ $p < 0.01$, $***$ $p < 0.001$ versus control; # $p < 0.05$, ## $p < 0.01$ versus CP 5 μM; $ $p < 0.05$, $$ $p < 0.01$, $$$ $p < 0.001$ versus CP 10 μM. CP: cisplatin; *p16:* cyclin-dependent kinase inhibitor 2A; *p21:* cyclin-dependent kinase inhibitor 1A; *p27:* cyclin-dependent kinase inhibitor 1B; *MMP3:* matrix metalloproteinase-3; *TNF-α:* tumor necrosis factor alpha; βOHB: β-hydroxybutyrate; *ɣ-H2AX:* gamma-H2A.X variant histone.
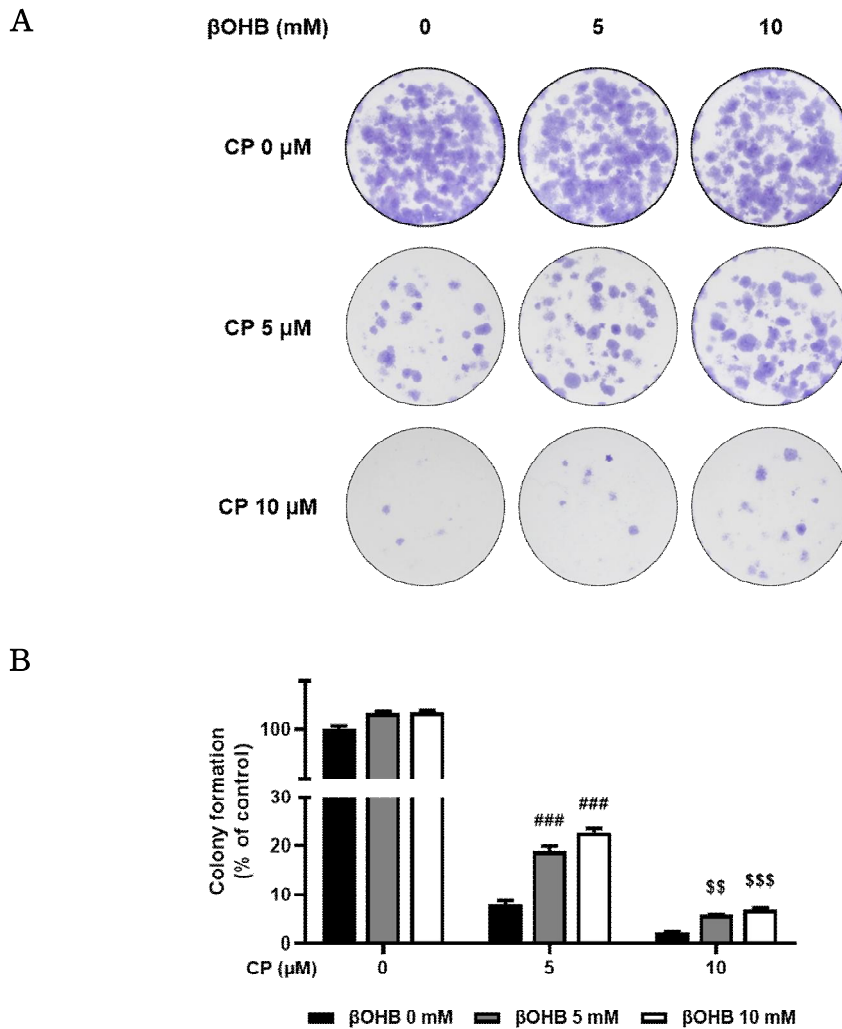
A

B

Figure 7. Effect of βOHB on colony formation in CP-treated HK-2 cells. HK-2 cells were induced with CP (5 or 10 μM) for 6 hours and then replaced with medium containing βOHB (5 or 10 mM) and cultured for 7 days. **(A)** Representative results of the colony formation assay in HK-2 cells were stained with crystal violet. **(B)** A quantitative analysis of the colony numbers was performed using Image J. Data are the mean ± SD. Experiments were performed at least three times

independently. Significant differences are indicated: ### $p <$ 0.001 versus CP 5 μM; \$\$ $p < 0.01$, \$\$\$ $p < 0.001$ versus CP 10 μM. CP: cisplatin; βOHB: β-hydroxybutyrate.
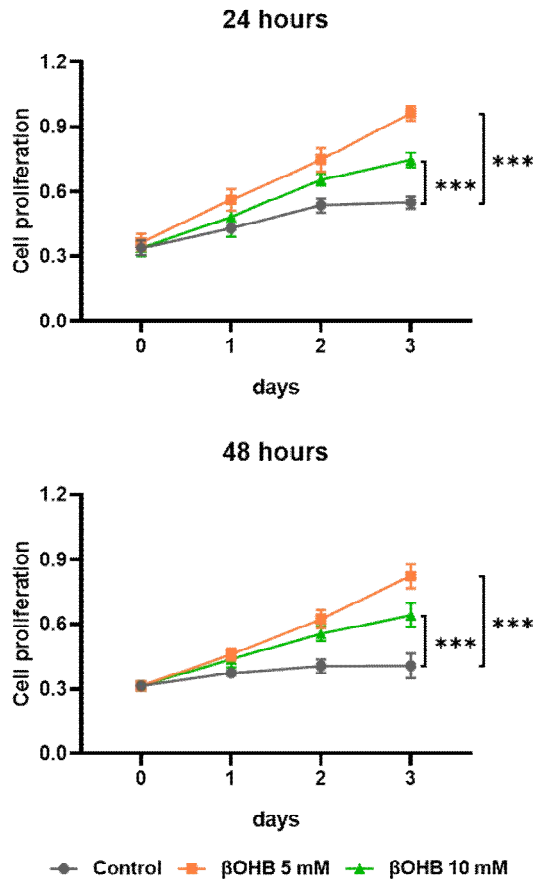
Figure 8. Effect of βOHB on cell proliferation in CP-treated HK-2 cells. Cell proliferation assays were performed daily for 3 days using the CCK-8. HK-2 cells were incubated with CP at 5 μM for 24 and 48 hours of treatment, followed by replacement with medium containing βOHB (5 or 10 mM). The top panel is 24 hours CP-induction, and the bottom panel is 48 hours CP-induction. Data are the mean ± SD. Experiments were performed at least three times independently. *** $p < 0.001$ versus control. CCK-8: Cell Counting Kit-8; CP: cisplatin; βOHB: β-hydroxybutyrate.
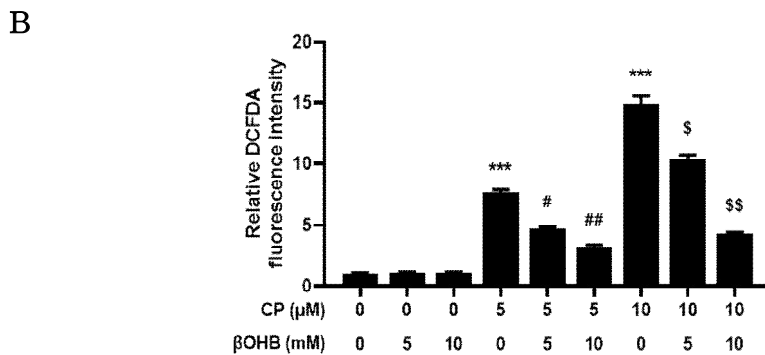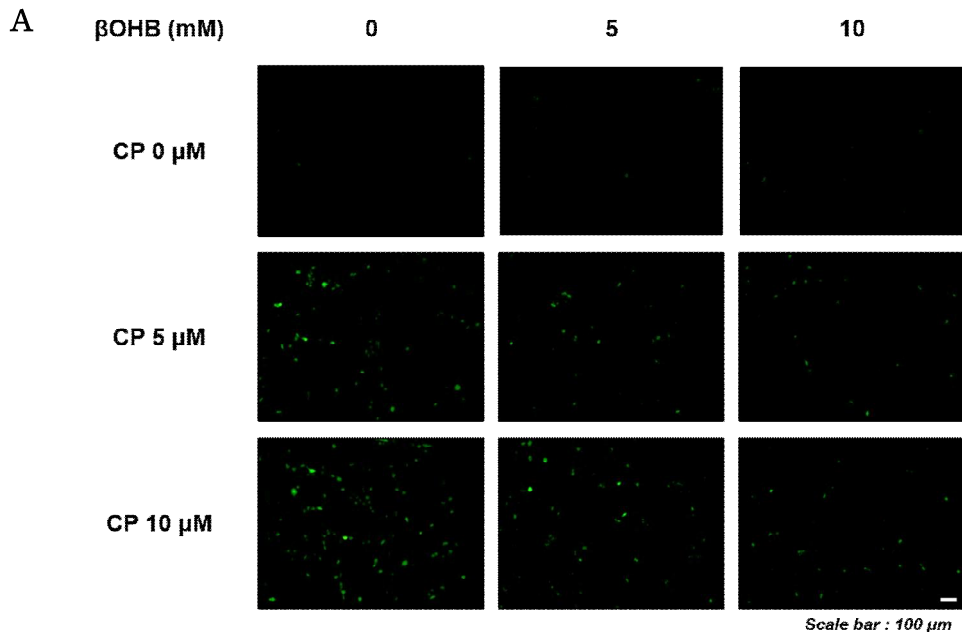
A

B

Figure 9. Effect of βOHB on CP-induced ROS production in HK-2 cells. HK-2 cells were pre-incubated with different concentrations of βOHB (5 or 10 mM) for 2 hours before treatment with different concentrations of CP (5 or 10 μM) for 30 minutes. **(A)** Images of the DCFDA staining were captured under a fluorescence microscopy (original magnification × 10; scale bar = 100 μm). **(B)** Quantitative fluorescence

intensities of DCFDA staining were analyzed using Image J. Data are the mean ± SD. Experiments were performed at least three times independently. Significant differences are indicated: *** $p < 0.001$ versus control; # $p < 0.05$, ## $p < 0.01$ versus CP 5 μM; $ $p < 0.05$, $$ $p < 0.01$ versus CP 10 μM. CP: cisplatin; DCFDA: 2',7'-dichlorofluorescein diacetate; ROS: reactive oxygen species; βOHB: β-hydroxybutyrate.
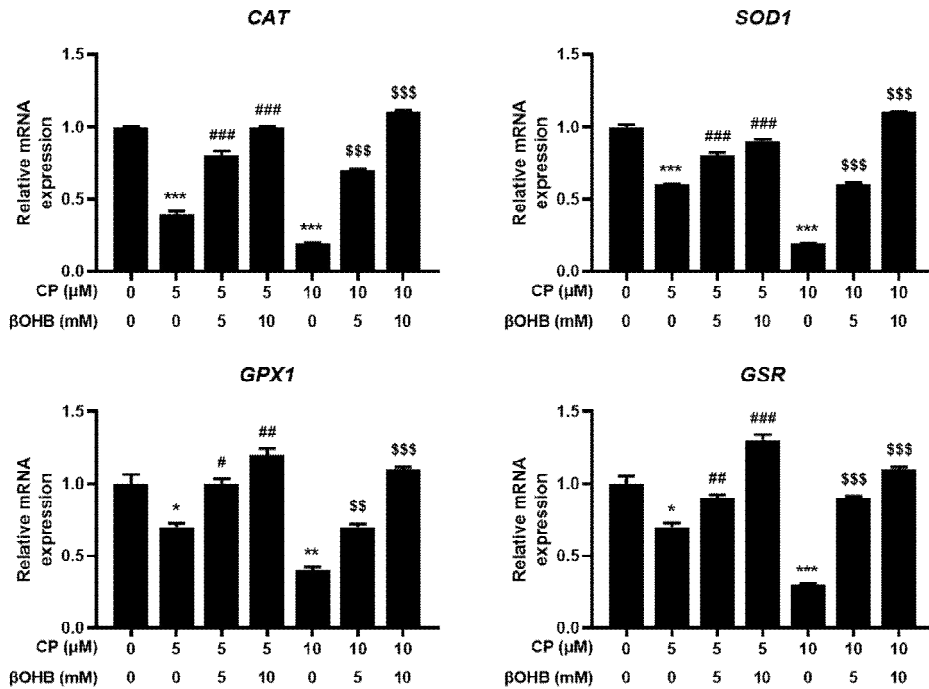
Figure 10. Analysis of ROS scavenger gene expression with βOHB in CP-treated HK-2 cells. HK-2 cells were pre-incubated with different concentrations of βOHB (5 or 10 mM) for 2 hours before treatment with different concentrations of CP (5 or 10 μM) for 30 minutes. Real-time PCR analysis of ROS scavenger markers (*CAT, SOD1, GPX1, and GSR*) in HK-2 cells. Data are the mean ± SD. Experiments were performed at least three times independently. Significant differences are indicated: $*$ $p < 0.05$, $**$ $p < 0.01$, $***$ $p < 0.001$ versus control; # $p < 0.05$, ## $p < 0.01$, ### $p < 0.001$ versus CP 5 μM; \$\$ $p < 0.01$, \$\$\$ $p < 0.001$ versus CP 10 μM. *CAT:* catalase; CP: cisplatin; *GPX1:* glutathion peroxidase 1; *GSR:* glutathione reductase; ROS: reactive oxygen species; *SOD1:* superoxide dismutase; βOHB: β-hydroxybutyrate.

A βOHB (100 mg/kg) daily i.p.

C57BL/6 mice (8-wk-old male)

0 1 2 3 4 5 6 7 Days

CP (25 mg/kg) single i.p.   Sampling

CTL
β-hydroxybutyrate (βOHB)
Cisplatin (CP)
βOHB + CP

B Control βOHB CP βOHB + CP

Scale bar : 1.5 mm

C Control βOHB CP βOHB + CP
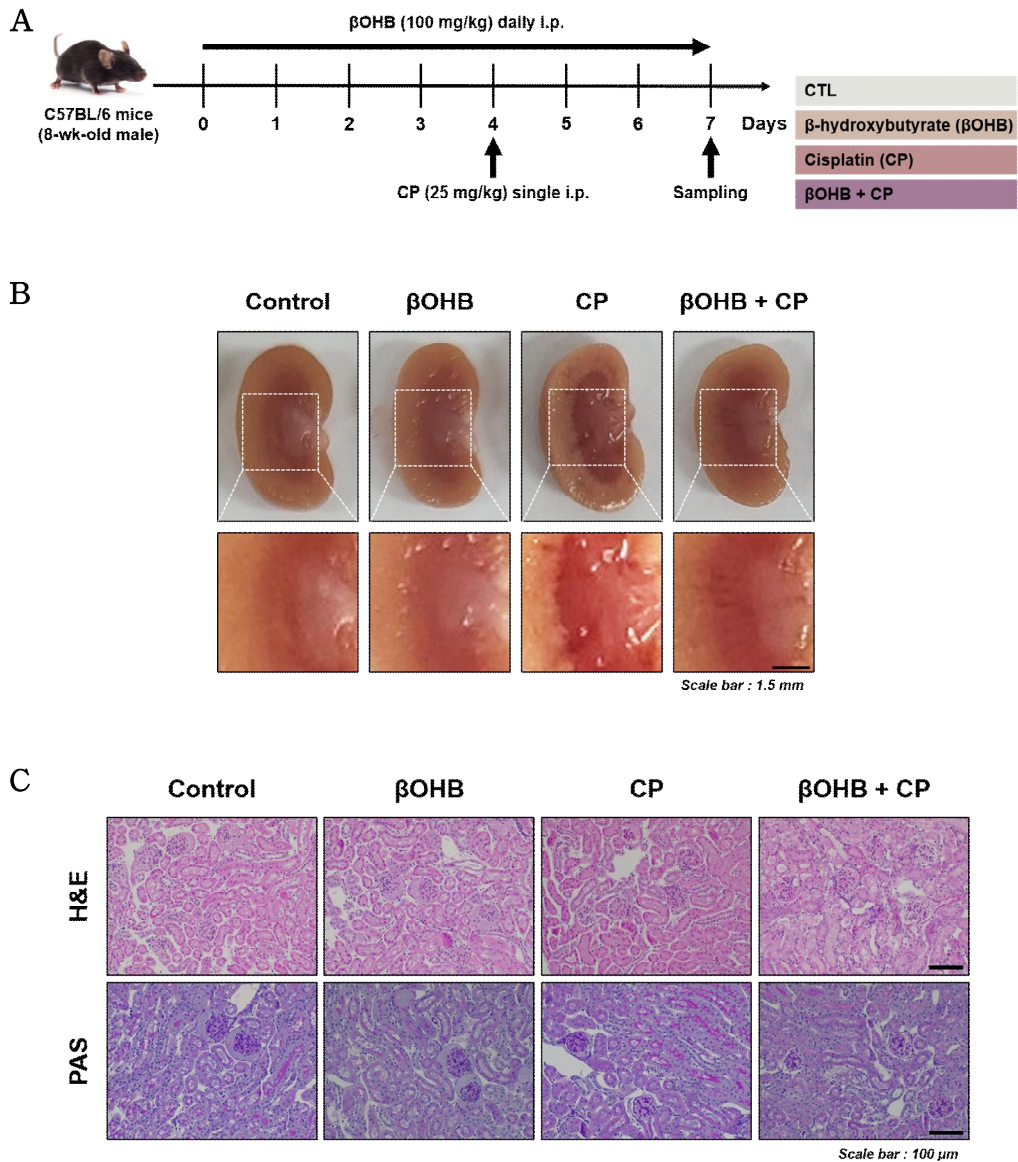
H&E

PAS

Scale bar : 100 μm

Figure 11. CP-induced AKI is inhibited by βOHB. (A) Representative schematic of the *in vivo* experiment using the CP-induced AKI model in combination with βOHB. **(B)** Kidney morphology (scale bar = 1.5 mm). **(C)** Representative images of H&E staining and PAS staining of CP-induced

AKI mice kidneys were observed under light microscopy (original magnification × 20; scale bar = 100 μm). AKI: acute kidney injury; CP: cisplatin; H&E: hematoxylin and eosin; i.p.: intraperitoneal; PAS: periodic acid-Schiff; βOHB: β-hydroxybutyrate.
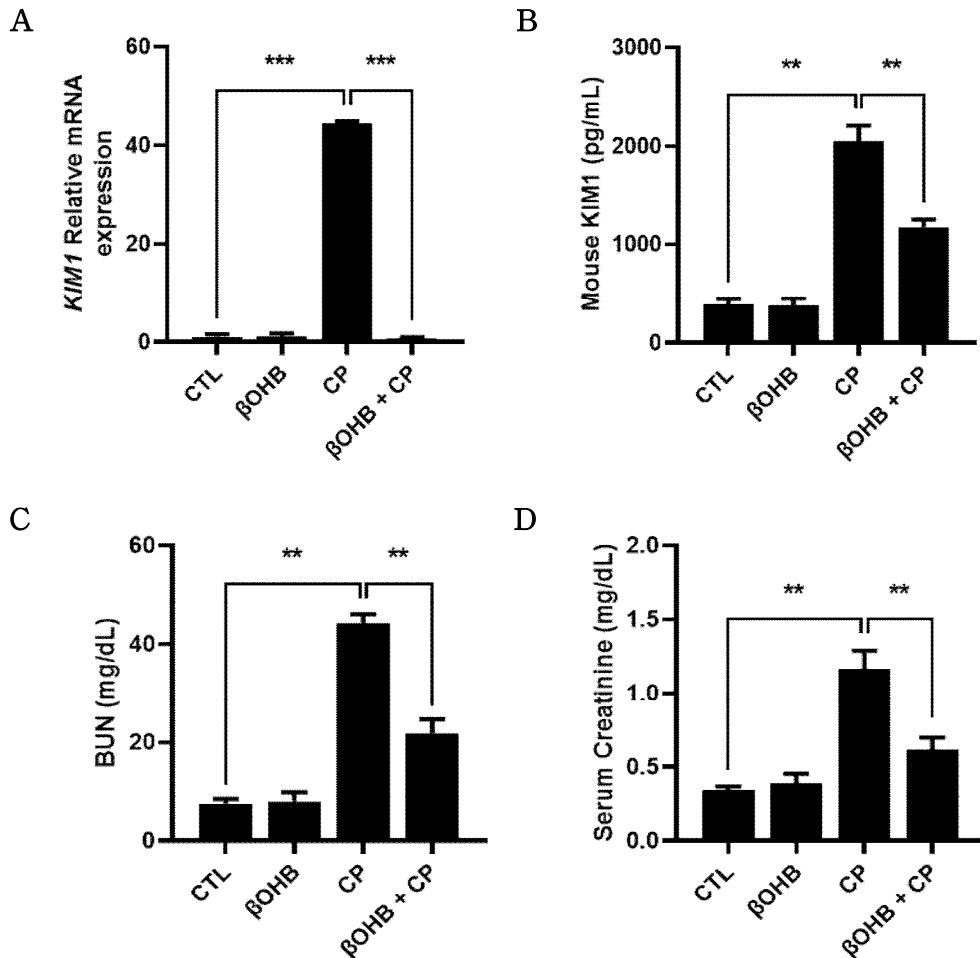
Figure 12. Effect of βOHB on kidney function in CP-induced AKI mice. (A) mRNA expression of the kidney injury marker *KIM1* was measured by real-time PCR. Serum KIM1 (B), BUN (C), and SCr (D) were measured by ELISA. Data are the mean ± SD. ** $p < 0.01$, *** $p < 0.001$. AKI: acute kidney injury; BUN: blood urea nitrogen; CP: cisplatin; ELISA: enzyme-linked immunosorbent assay; *KIM1:* kidney injury molecule 1; SCr: serum creatinine; βOHB: β-hydroxybutyrate.
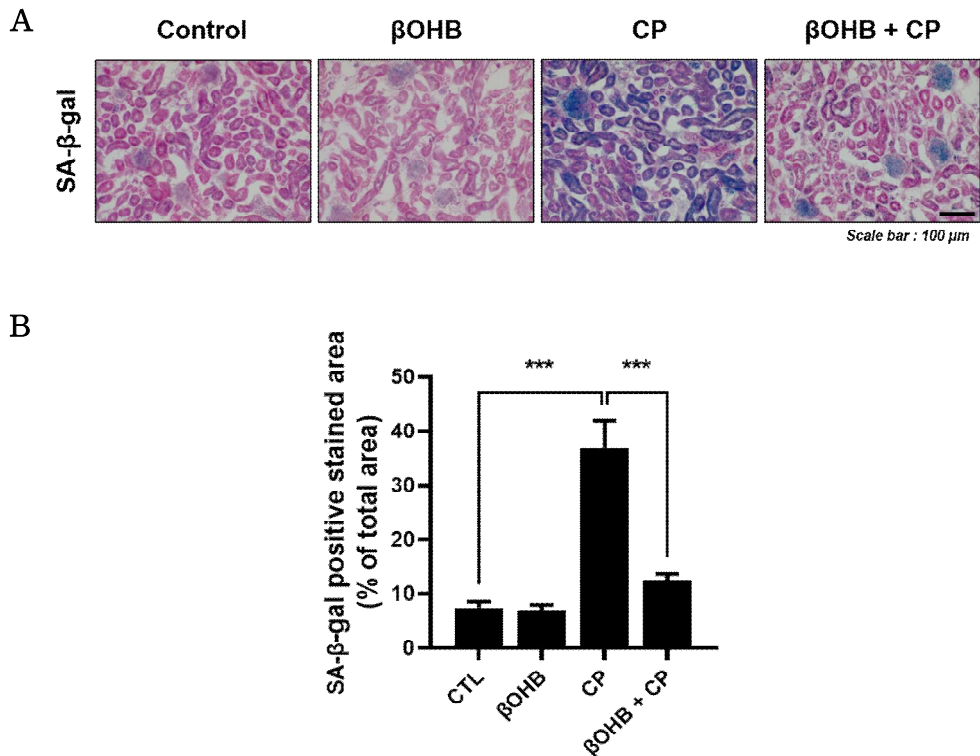
Figure 13. Analysis of the anti-senescence effect of βOHB in CP-
induced AKI mice. (A) Representative light microscopy
images of SA-β-gal staining in the kidney of CP-induced
AKI mice (original magnification × 20; scale bar = 100 μm).
(B) Cellular senescence was quantified as the positive area
of SA-β-gal staining (blue) was analyzed using Image J.
Data are the mean ± SD. *** $p < 0.001$. AKI: acute kidney
injury; CP: cisplatin; SA-β-gal: senescence-associated β
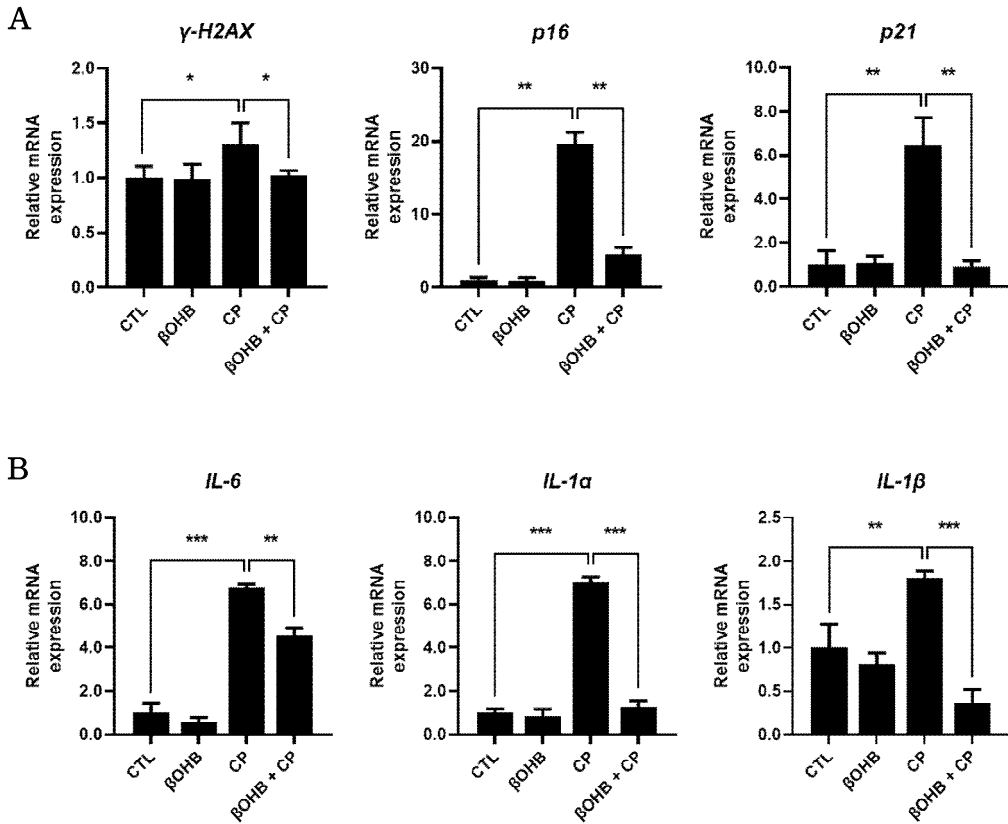-galactosidase; βOHB: β-hydroxybutyrate.

A

B

Figure 14. Analysis of senescence and SASP gene expression with βOHB in CP-induced AKI mice. Real-time PCR analysis of senescence markers (*H2AX, p16,* and *p21*) (**A**) and SASP markers (*IL-6, IL-1a,* and *IL-1β*) (**B**) in the kidney of CP-induced AKI mice. Data are the mean ± SD. Experiments were performed at least three times independently. $* p < 0.05$, $** p < 0.01$, $*** p < 0.001$. AKI: acute kidney injury; CP: cisplatin; *IL-1a:* interleukin-1 alpha; *IL-1β:* interleukin-1 beta; *IL-6:* interleukin 6; *p16:* cyclin-dependent kinase inhibitor 2A; *p21:* cyclin-dependent kinase inhibitor 1A; SASP: senescence-associated secretory

phenotype; βOHB: β-hydroxybutyrate; *ɣ-H2AX:* gamma-H2A.X variant histone.

A

	Control	βOHB	CP	βOHB + CP

DAPI

DHE

Merge

Scale bar : 100 μm

B

D

C

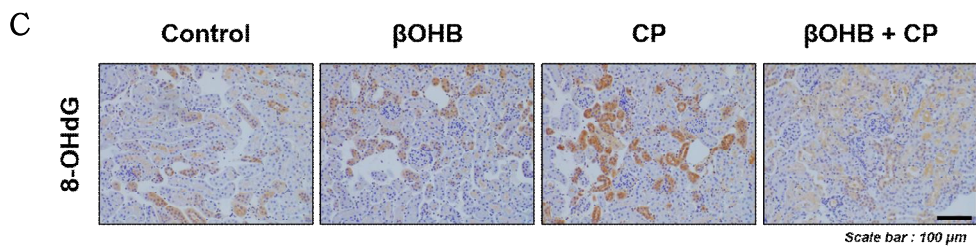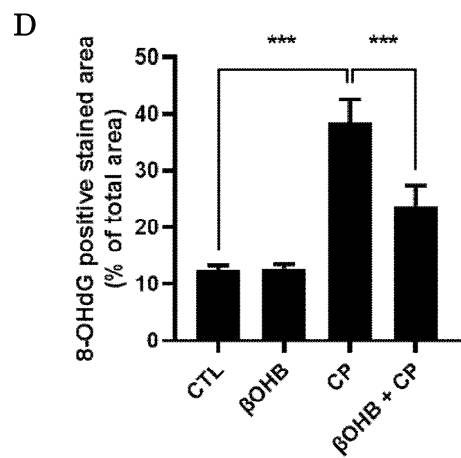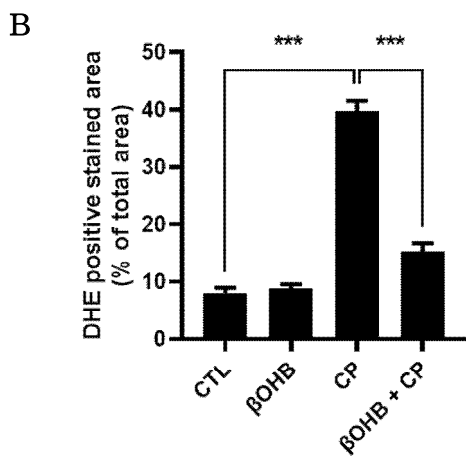|	Control	βOHB	CP	βOHB + CP

8-OHdG
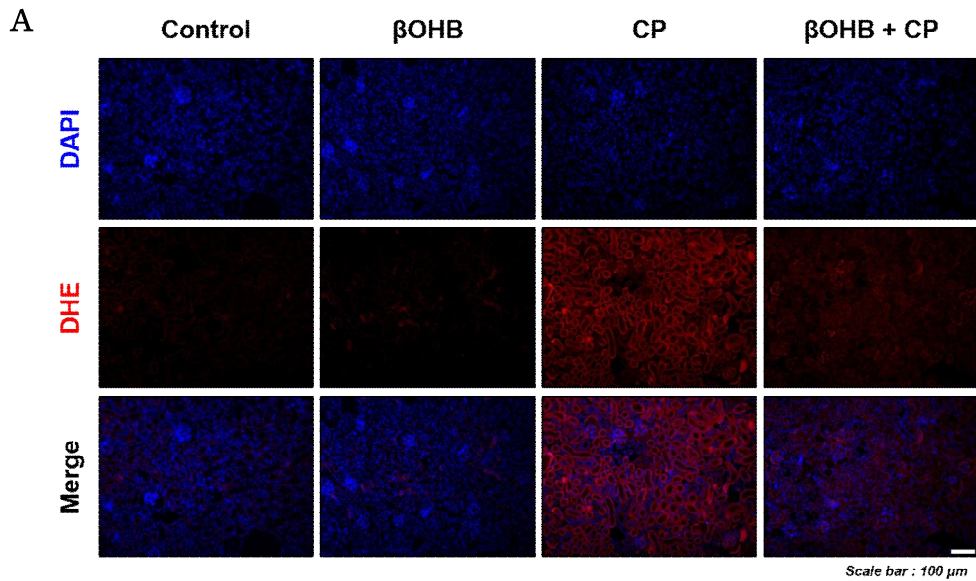
Scale bar : 100 μm

Figure 15. Expression of oxidative stress markers in the kidney of CP-induced AKI mice. (A) Representative fluorescence microscopy images of DHE staining in the kidney of CP-induced AKI mice (original magnification × 20; scale bar = 100 μm). (B) A quantitative fluorescence positive area of DHE staining (red) was analyzed using Image J. (C) IHC evaluation of 8-OHdG expression in CP-induced AKI mice was observed by light microscopy (original magnification × 20; scale bar = 100 μm). (D) The graphs show the results of the quantitative analysis of 8-OHdG, which was analyzed with Image J. Data are the mean ± SD. *** $p < 0.001$. AKI: acute kidney injury; CP: cisplatin; DAPI: 4′,6-diamidino-2-pheylindole; DHE: dihydroethidium; IHC: immunohistochemistry; βOHB: β-hydroxybutyrate; 8-OHdG: 8-hydrox-2-deoxyguanosine.
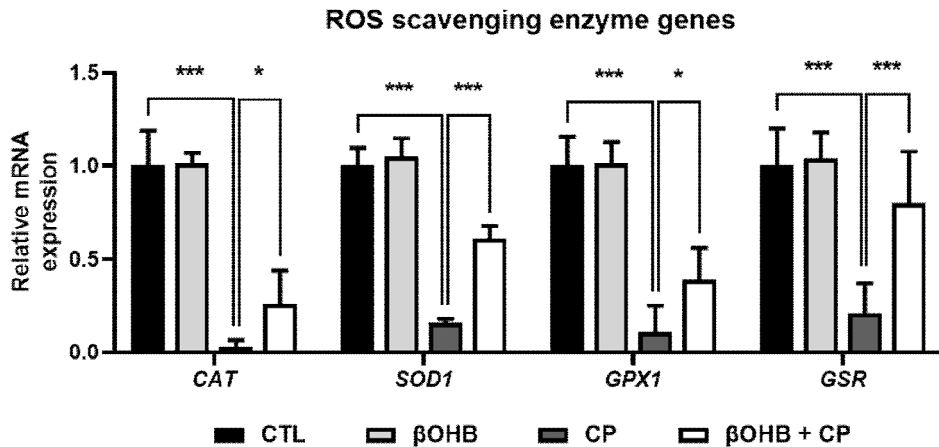
Figure 16. Analysis of the expression of ROS scavenger genes in the kidney of CP-induced AKI mice. Real-time PCR analysis of ROS scavenger markers (*CAT, SOD1, GPX1, and GSR*) in CP-induced AKI mice. Data are the mean ± SD. Experiments were performed at least three times independently. $*$ $p < 0.05$, $***$ $p < 0.001$. AKI: acute kidney injury; *CAT:* catalase; CP: cisplatin; *GPX1:* glutathion peroxidase 1; *GSR:* glutathione reductase; ROS: reactive oxygen species; *SOD1:* superoxide dismutase; βOHB: β-hydroxybutyrate.

Figure 17. Schematic illustration of the main results of this study. CP-induced increased apoptosis, senescence, and decreased proliferation were attenuated by βOHB to attenuate AKI. A reduction in ROS was associated with these effects. AKI: acute kidney injury; CP: cisplatin; ROS: reactive oxygen species; βOHB: β-hydroxybutyrate.

4. Discussion

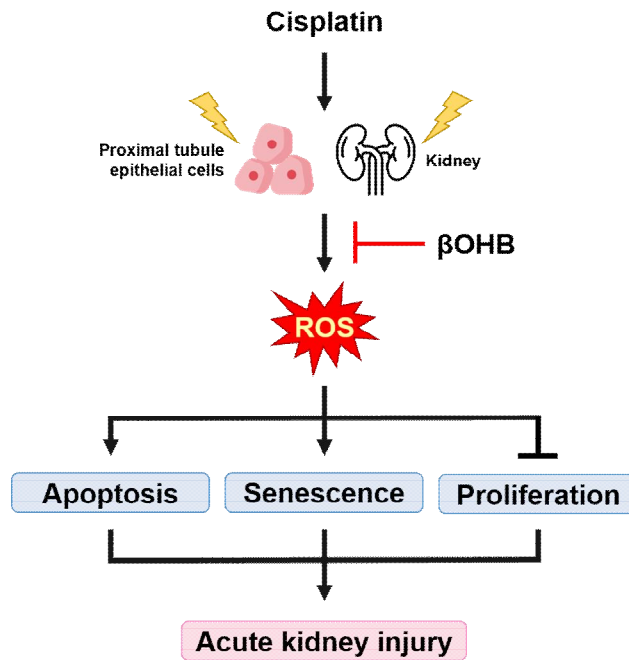This study shows the potential therapeutic effects of βOHB on *in vitro* and *in vivo* models of CP-induced AKI by showing that βOHB protects the kidney against CP-induced apoptosis, senescence, and proliferation, possibly by inhibiting ROS production.

βOHB is one of the ketone bodies that the liver produces. βOHB concentrations increase in the brain, liver, and other tissues during fasting, CR, exercise, and ketogenic diets. There is evidence that βOHB can be used to treat numerous diseases (46 - 49). The ketogenic diet, which consists primarily of βOHB, is an important treatment for intractable childhood epilepsy (50). βOHB is neuroprotective against Parkinson's and Alzheimer's diseases in the hippocampus (51). In addition, the ketogenic diet reduces obesity and diabetes effectively and delays the aging process (52). Administration of βOHB is highly protective of the brain, heart, liver, and kidney in rodents (32), and a diet supplemented with βOHB extends the lifespan of mice, suggesting an advantageous dietary strategy for preventing age-associated dysfunction (53).

CP causes premature kidney senescence and progressive renal fibrosis, which leads to macromolecular damage, pro-inflammatory SASPs, and higher levels of cell cycle inhibitors (including p16 and p21), SA-β-gal activity, and ɣ-H2AX (54 - 56). This study demonstrated that βOHB inhibits senescence in kidney tissue and CP-induced tubular epithelial cells. βOHB treatment decreased CP-induced SA-β-gal staining, a well-established senescence marker (Figure 5&13). In addition, βOHB inhibited CP-stimulated senescence and SASP gene expression (Figure 6&14). The findings of this study are consistent with recent research

showing that a CR or ketogenic diet reduces CP-induced senescence by upregulating βOHB (35).

As shown by *in vitro* data (Figure 3&4), βOHB has a direct protective effect against tubular cell injury. It is well documented that a single high-dose CP (20‑30 mg/kg body weight) injected into mice induces significant kidney damage manifested by cell death, necrosis, and renal dysfunction (57,58). In this study, CP treatment at 25 mg/kg significantly increased the mRNA levels of *KIM1*, a marker of kidney dysfunction, in the kidney tissue (Figure 12A), as well as the serum levels of BUN, SCr, and KIM1 (Figure 12B‑D). In contrast, treatment with βOHB inhibited the expression of kidney dysfunction markers. This *in vivo* evidence strongly suggests that βOHB could be used as a treatment for CP-induced nephrotoxicity. However, further studies are needed to determine the direct effects and the mechanisms underlying βOHB on CP-induced renal tubular cell injury.

AKI is a rapid decrease in kidney function that includes changes in SCr, BUN, and urine volume. AKI is frequently caused by sepsis, cardiovascular disease, major surgery, toxins, or urinary outflow obstruction, resulting in severe morbidity and mortality (59,60). It is also known that complications from AKI, particularly the likelihood of AKI progressing to chronic kidney disease (CKD), increases considerably with age (61). Despite its clinical importance, a lack of targeted therapies limits the treatment of AKI, resulting in a high mortality rate among patients with AKI. The results of this study suggest that βOHB as a nutritional intervention may be a promising therapeutic strategy for the prevention of AKI.

The evidence suggests that oxidative stress is a key player in the pathogenesis of CP-induced nephrotoxicity (12). Figure 9 and 15 demonstrate that βOHB significantly decreases oxidative stress by

decreasing ROS production in CP-induced HK-2 cells and kidney tissue. In addition, antioxidant enzymes were decreased by CP and increased by βOHB treatment, showing the mechanism underlying βOHB ability to decrease CP-induced nephrotoxicity (Figure 10&16).

In conclusion, Figure 17 demonstrates that βOHB may ameliorate CP-induced AKI by inhibiting apoptosis, cellular senescence, and proliferation by decreasing ROS production. This provides new evidence that βOHB-induced inhibition of ROS decreases CP-induced kidney injury, mortality, and senescence and suggests that βOHB may prevent CP-induced AKI in humans.

5. Summary

The aim of this study is to determine whether βOHB is able to alleviate the side effects of CP-induced AKI. Analyses of cell viability, cytotoxicity, and apoptosis gene expression showed that βOHB protects human proximal tubule epithelial cell lines (HK-2) from CP-induced apoptosis. Moreover, SA-β-gal staining and measurements of senescence and SASP gene expression demonstrated that βOHB inhibited CP-induced cellular senescence. As confirmed by colony formation and cell proliferation assays, βOHB increased the cell proliferation that CP had inhibited. In addition, DCFDA staining and analysis of antioxidant gene expression demonstrated that βOHB inhibited CP-induced ROS production. In an animal model of CP-induced AKI, βOHB significantly decreased serum concentrations of KIM1, BUN, and SCr. In addition, βOHB inhibited cellular senescence in CP-induced AKI, as determined by SA-β-gal staining, kidney tissue senescence, and SASP gene expression. As a result, βOHB inhibited increased ROS production in CP-induced AKI linked to DHE staining, 8-OHdG IHC, and antioxidant gene expression in kidney tissue.

References

1. Florea A-M, Büsselberg D: Cisplatin as an anti-tumor drug: cellular mechanisms of activity, drug resistance and induced side effects. Cancers (Basel) 2011; 3(1): 1351-71.

2. Choi Y-M, Kim H-K, Shim W, Anwar MA, Kwon J-W, Kwon H-K, et al: Mechanism of Cisplatin-Induced Cytotoxicity Is Correlated to Impaired Metabolism Due to Mitochondrial ROS Generation. PLoS One 2015; 10(8): 0135083.

3. Alassaf N, Attia H: Autophagy and necroptosis in cisplatin-induced acute kidney injury: Recent advances regarding their role and therapeutic potential. Front Pharmacol 2023; 14: 1103062.

4. Safirstein R, Winston J, Goldstein M, Moel D, Dikman S, Guttenplan J: Cisplatin Nephrotoxicity. Am J Kidney Dis 1986; 8(5): 356-67.

5. Arany I, Safirstein RL: Cisplatin nephrotoxicity. Semin Nephrol 2003; 23(5): 460-4.

6. Yao X, Panichpisal K, Kurtzman N, Nugent K: Cisplatin Nephrotoxicity: A Review. Am J Med Sci 2007; 334(2): 115-24.

7. Pabla N, Dong Z: Cisplatin nephrotoxicity: Mechanisms and renoprotective strategies. Kidney Int 2008; 73(9): 994-1007.

8. Miller RP, Tadagavadi RK, Ramesh G, Reeves WB: Mechanisms of

Cisplatin Nephrotoxicity. Toxins 2010; 2(11): 2490−518.

9. Ozkok A, Edelstein CL: Pathophysiology of cisplatin-induced acute kidney injury. Biomed Res Int 2014; 2014: 967826.

10. Sato K, Watanabe S, Ohtsubo A, Shoji S, Ishikawa D, Tanaka T, et al: Nephrotoxicity of cisplatin combination chemotherapy in thoracic malignancy patients with CKD risk factors. BMC Cancer 2016; 16: 222.

11. Holditch SJ, Brown CN, Lombardi AM, Nguyen KN, Edelstein CL: Recent Advances in Models, Mechanisms, Biomarkers, and Interventions in Cisplatin-Induced Acute Kidney Injury. Int J Mol Sci 2019; 20(12): 3011.

12. McSweeney KR, Gadanec LK, Qaradakhi T, Ali BA, Zulli A, Apostolopoulos V: Mechanisms of Cisplatin-Induced Acute Kidney Injury: Pathological Mechanisms, Pharmacological Interventions, and Genetic Mitigations. Cancers (Basel) 2021; 13(7): 1572.

13. Turgut F, Awad AS, Abdel-Rahman EM: Acute Kidney Injury: Medical Causes and Pathogenesis. J Clin Med 2023; 12(1): 375.

14. Liu H, Yan L-J: The Role of Ketone Bodies in Various Animal Models of Kidney Disease. Endocrines 2023; 4(1): 236–49.

15. Negi S, Koreeda D, Kobayashi S, Yano T, Tatsuta K, Mima T, et al: Acute kidney injury: Epidemiology, outcomes, complications, and therapeutic strategies. Semin Dial 2018; 31(5): 519–27.

16. Sears SM, Dupre TV, Shah PP, Davis DL, Doll MA, Sharp CN, et al: Neutral ceramidase deficiency protects against cisplatin-induced acute kidney injury. J Lipid Res 2022; 63(3): 100179.

17. Touyz RM: Molecular and cellular mechanisms in vascular injury in hypertension: role of angiotensin II. Curr Opin Nephrol Hypertens 2005; 14(2): 125-31.

18. Mueller CF, Laude K, McNally JS, Harrison DG: Redox Mechanisms in Blood Vessels. Arterioscler Thromb Vasc Biol 2005; 25(2): 274-8.

19. Abdal Dayem A, Hossain MK, Lee SB, Kim K, Saha SK, Yang G-M, et al: The Role of Reactive Oxygen Species (ROS) in the Biological Activities of Metallic Nanoparticles. Int J Mol Sci 2017; 18(1): 120.

20. Meng X-M, Ren G-L, Gao L, Yang Q, Li H-D, Wu W-F, et al: NADPH oxidase 4 promotes cisplatin-induced acute kidney injury via ROS-mediated programmed cell death and inflammation. Lab Invest 2018; 98(1): 63-78.

21. Reyes-Fermín LM, Avila-Rojas SH, Aparicio-Trejo OE, Tapia E, Rivero I, Pedraza-Chaverri J: The Protective Effect of Alpha-Mangostin against Cisplatin-Induced Cell Death in LLC-PK1 Cells is Associated to Mitochondrial Function Preservation. Antioxidants (Basel) 2019; 8(5): 133.

22. Kim J-Y, Jo J, Leem J, Park K-K: Inhibition of p300 by Garcinol

Protects against Cisplatin-Induced Acute Kidney Injury through Suppression of Oxidative Stress, Inflammation, and Tubular Cell Death in Mice. Antioxidants (Basel) 2020; 9(12): 1271.

23. Kerr JF, Wyllie AH, Currie AR: Apoptosis: A basic biological phenomenon with wide-ranging implications in tissue kinetics. Br J Cancer 1972; 26(4): 239-57.

24. Fulda S, Gorman AM, Hori O, Samali A: Cellular stress responses: cell survival and cell death. Int J Cell Biol 2010; 2010: 214074.

25. Redza-Dutordoir M, Averill-Bates DA: Activation of apoptosis signalling pathways by reactive oxygen species. Biochim Biophys Acta 2016; 1863(12): 2977-92.

26. Patel R, Rinker L, Peng J, Chilian WM: Reactive Oxygen Species: The Good and the Bad. Reactive Oxygen Species (ROS) in Living Cells 2018; 7.

27. Han Y-M, Bedarida T, Ding Y, Somba BK, Lu Q, Wang Q, et al: β-Hydroxybutyrate Prevents Vascular Senescence through hnRNP A1-Mediated Upregulation of Oct4. Mol Cell 2018; 71(6): 1064-78.

28. Han Y-M, Ramprasath T, Zou M-H: β-hydroxybutyrate and its metabolic effects on age-associated pathology. Exp Mol Med 2020; 52(4): 548-55.

29. Ristow M, Schmeisser S: Extending life span by increasing oxidative stress. Free Radic Biol Med 2011; 51(2): 327-36.

30. Sergiev PV, Dontsova OA, Berezkin GV: Theories of aging: an ever-evolving field. Acta Naturae 2015; 7(1): 9-18.

31. Davalli P, Mitic T, Caporali A, Lauriola A, D'Arca D: ROS, Cell Senescence, and Novel Molecular Mechanisms in Aging and Age-Related Diseases. Oxid Med Cell Longev 2016; 2016: 3565127.

32. Rojas-Morales P, Pedraza-Chaverri J, Tapia E: Ketone bodies, stress response, and redox homeostasis. Redox Biol 2020; 29: 101395.

33. Kolb H, Kempf K, Röhling M, Lenzen-Schulte M, Schloot NC, Martin S: Ketone bodies: from enemy to friend and guardian angel. BMC Med 2021; 19(1): 313.

34. Wang L, Chen P, Xiao W: β-hydroxybutyrate as an Anti-Aging Metabolite. Nutrients 2021; 13(10): 3420.

35. Luo S, Yang M, Han Y, Zhao H, Jiang N, Li L, et al: β-Hydroxybutyrate against Cisplatin-Induced acute kidney injury via inhibiting NLRP3 inflammasome and oxidative stress. Int Immunopharmacol 2022; 111: 109101.

36. Roberts MN, Wallace MA, Tomilov AA, Zhou Z, Marcotte GR, Tran D, et al: A Ketogenic Diet Extends Longevity and Healthspan in Adult Mice. Cell Metab 2017; 26(3): 539-46.

37. Edwards C, Copes N, Bradshaw PC: D-ß-hydroxybutyrate: an anti-aging ketone body. Oncotarget 2015; 6(6): 3477-8.

38. Veech RL, Bradshaw PC, Clarke K, Curtis W, Pawlosky R, King MT: Ketone bodies mimic the life span extending properties of caloric restriction. IUBMB Life 2017; 69(5): 305-14.

39. Rojas-Morales P, Tapia E, Pedraza-Chaverri J: β-Hydroxybutyrate: A signaling metabolite in starvation response? Cell Signal 2016; 28(8): 917-23.

40. Tajima T, Yoshifuji A, Matsui A, Itoh T, Uchiyama K, Kanda T, et al: β-hydroxybutyrate attenuates renal ischemia-reperfusion injury through its anti-pyroptotic effects. Kidney Int 2019; 95(5): 1120-37.

41. Mizobata Y, Hiraide A, Katayama M, Sugimoto H, Yoshioka T, Sugimoto T: Oxidation of D(-)3-hydroxybutyrate administered to rats with extensive burns. Surg Today 1996; 26(3): 173-8.

42. Hiraide A, Katayama M, Mizobata Y, Sugimoto H, Yoshioka T, Sugimoto T: Effect of sodium D-3-hydroxybutyrate on amino acidemia in hemorrhagic hypotension. Eur Surg Res 1991; 23(3-4): 250-5.

43. Katayama M, Hiraide A, Sugimoto H, Yoshioka T, Sugimoto T: Effect of ketone bodies on hyperglycemia and lactic acidemia in hemorrhagic stress. JPEN J Parenter Enteral Nutr 1994; 18(5): 442-6.

44. Suzuki M, Suzuki M, Sato K, Dohi S, Sato T, Matsuura A, et al: Effect of β-hydroxybutyrate, a cerebral function improving agent, on cerebral hypoxia, anoxia and ischemia in mice and rats. Jpn J

Pharmacol 2001; 87(2): 143–50.

45. Dimri GP, Lee X, Basile G, Acosta M, Scott G, Roskelley C, et al: A biomarker that identifies senescent human cells in culture and in aging skin in vivo. Proc Natl Acad Sci U S A 1995; 92(20): 9363–7.

46. Newman JC, Verdin E: Ketone bodies as signaling metabolites. Trends Endocrinol Metab 2014; 25(1): 42–52.

47. Newman JC, Verdin E: β-Hydroxybutyrate: A Signaling Metabolite. Annu Rev Nutr 2017; 37: 51–76.

48. Puchalska P, Crawford PA: Multi-dimensional Roles of Ketone Bodies in Fuel Metabolism, Signaling, and Therapeutics. Cell Metab 2017; 25(2): 262–84.

49. Rojas-Morales P, Pedraza-Chaverri J, Tapia E: Ketone bodies for kidney injury and disease. Adv Redox Res 2021; 2: 100009.

50. Simeone TA, Simeone KA, Rho JM: Ketone Bodies as Anti-Seizure Agents. Neurochem Res 2017; 42(7): 2011–8.

51. Kashiwaya Y, Takeshima T, Mori N, Nakashima K, Clarke K, Veech RL: D-beta-hydroxybutyrate protects neurons in models of Alzheimer's and Parkinson's disease. Proc Natl Acad Sci U S A 2000; 97(10): 5440–4.

52. Fang Y, Chen B, Gong AY, Malhotra DK, Gupta R, Dworkin LD, et al: The ketone body β-hydroxybutyrate mitigates the senescence

response of glomerular podocytes to diabetic insults. Kidney Int 2021; 100(5): 1037–53.

53. Fan SZ, Lin CS, Wei YW, Yeh SR, Tsai YH, Lee AC, et al: Dietary citrate supplementation enhances longevity, metabolic health, and memory performance through promoting ketogenesis. Aging Cell 2021; 20(12): 13510.

54. Li C, Xie N, Li Y, Liu C, Hou FF, Wang J: N-acetylcysteine ameliorates cisplatin-induced renal senescence and renal interstitial fibrosis through sirtuin1 activation and p53 deacetylation. Free Radic Biol Med 2019; 130: 512–27.

55. Li Y, Lerman LO: Cellular Senescence: A New Player in Kidney Injury. Hypertension 2020; 76(4): 1069–75.

56. Sears SM, Siskind LJ: Potential Therapeutic Targets for Cisplatin-Induced Kidney Injury: Lessons from Other Models of AKI and Fibrosis. J Am Soc Nephrol 2021; 32(7): 1559–67.

57. Perše M, Večerić-Haler Ž: Cisplatin-Induced Rodent Model of Kidney Injury: Characteristics and Challenges. Biomed Res Int 2018; 2018: 1462802.

58. Perše M: Cisplatin Mouse Models: Treatment, Toxicity and Translatability. Biomedicines 2021; 9(10): 1406.

59. Hoyer-Allo KJR, Späth MR, Brodesser S, Zhu Y, Binz-Lotter J, Höhne M, et al: Caloric restriction reduces the pro-inflammatory

eicosanoid 20-hydroxyeicosatetraenoic acid to protect from acute kidney injury. Kidney Int 2022; 102(3): 560-76.

60. Koehler FC, Späth MR, Hoyer-Allo KJR, Müller R-U: Mechanisms of Caloric Restriction-Mediated Stress-Resistance in Acute Kidney Injury. Nephron 2022; 146(3): 234-8.

61. Andrianova NV, Zorova LD, Pevzner IB, Kolosova NG, Plotnikov EY, Zorov DB: Calorie Restriction Provides Kidney Ischemic Tolerance in Senescence-Accelerated OXYS Rats. Int J Mol Sci 2022; 23(23): 15224.

β-hydroxybutyrate Prevents Cellular Senescence and Apoptosis in Cisplatin-Induced Acute Kidney Injury

Kim, Mi Kyoung

Department of Biochemistry
Graduate School

Keimyung University

(Supervised by Professor Ha, Eun Young)

(Abstract)

Cisplatin (CP) is one of the most widely used and most effective chemotherapy drugs. However, the use of CP is limited by side effects, among which nephrotoxicity is the most important dose-dependent side effect. CP-induced nephrotoxicity is the accumulation of CP in the kidneys, causing renal tubular damage associated with cell death, inflammation, vascular damage, and oxidative and endoplasmic reticulum stress. Produced in the liver, β-hydroxybutyrate (βOHB) is a ketone body that acts as a metabolic fuel as well as an endogenous signaling molecule. Specifically, βOHB affects cellular processes by regulating intracellular pathways such as lipolysis, oxidative stress, histone methylation, and acetylation. The aim of this study is to determine the

potential effects of βOHB in protecting the kidney from the side effects of CP-induced acute kidney injury (AKI) and to investigate the underlying mechanisms. To accomplish the present study objectives, it was aimed to determine the role of βOHB in apoptosis, cellular senescence, and reactive oxygen species (ROS) production in CP-induced normal kidney cell lines and in a CP-induced AKI mouse model. In normal kidney cell lines, βOHB reduced CP-induced apoptosis and cellular senescence, and also decreased CP-induced ROS production. In a CP-induced AKI mouse model, levels of blood urea nitrogen (BUN), serum creatinine (SCr), and kidney injury molecule 1 (KIM1) were significantly reduced by βOHB-treatment, and cellular senescence and ROS expression were also reduced. In conclusion, this study has shown that βOHB provides renoprotection by reducing ROS production and oxidative stress in kidney injury. Further research is needed to determine whether βOHB may be a therapy for AKI treatment based on the results of this study.

β-hydroxybutyrate는 시스플라틴으로 유발된 급성 신장 손상에서 세포 노화 및 세포 사멸을 보호

김 미 경

계 명 대 학 교 대 학 원

의학과 생화학 전공

(지도교수 하 은 영)

(초록)

시스플라틴은 현재까지 가장 널리 사용되는 화학요법제이다. 시스플라틴에 의한 여러 부작용 중 신장에 미치는 부작용이 가장 강하고 크다. 따라서 이러한 신독성 부작용에 의해 시스플라틴 사용이 제한적이다. 시스플라틴에 의한 신독성은 시스플라틴이 신장에 집중적으로 축적됨으로써 세뇨관 손상을 일으키고, 이는 세포 사멸, 혈관 손상, 산화 및 소포체 스트레스, 염증과 관련되어있다. 간에서 생성되는 β-hydroxybutyrate (βOHB)는 케톤체 중 하나로써, 대사 연료 뿐만 아니라 내인성 신호 분자 물질로도 작용을 한다. 구체적으로, βOHB는 지방분해, 산화스트레스 억제, 신경보호 기능 향상, 히스톤 메틸화, 아세틸화 억제와 같은 세포 내 작용들을 조절하여 생리작용에 영향을 미친다. 본 연구는 시스플라틴에 의한 신장 손상 부작용을 βOHB가 완화시킬 수 있는 가에 대한 가능성을 검증하고 그 기전을 규명하는 것을 목적으로 한다. 연구 목적을 달성하기 위해서 시스플라틴으로 유도

된 정상 신장 세포주에서 세포 사멸, 세포 노화, 세포 주기 정지 및 활성산소종을 개선하는 βOHB의 역할을 확인하고, 시스플라틴으로 유도된 급성 신장 손상(acute kidney injury, AKI) 동물 모델에서 βOHB 의 신장 손상 보호 역할을 확인하고자 한다. 정상 신장 세포주에서 βOHB가 시스플라틴에 의해 증가 된 세포 사멸과 세포 노화를 감소시켰으며, 또한 시스플라틴에 의해 증가 된 활성산소종 발생을 감소시켰다. 시스플라틴에 의한 급성 신장 손상 동물 모델에서 신장 손상 분자(kidney injury molecule 1, KIM1)와 혈액 요소 질소(blood urea nitrogen, BUN) 및 혈청 크레아티닌(Creatinine, Cr)의 수치가 βOHB 처리에 의해 현저히 감소하였으며, 세포 노화 및 활성산소종의 발현도 감소하였다. 결과적으로, 본 연구는 βOHB가 신장 손상에서 활성산소종 생성과 산화스트레스를 감소시켜 신장을 보호하는 효과가 있음을 증명하였다. 본 연구 결과를 바탕으로 임상 AKI에서 βOHB가 치료제로 사용될 수 있는지에 대한 추가 연구가 필요하다.

□ 저자 약력

1990년 대구 출생

계명대학교 대학원 의학 석사

계명대학교 의과대학 생화학교실 박사학위 대학원생(현)

□ 논문 및 저서

「Changes in Glucose Transporters, Gluconeogenesis, and Circadian Clock after Duodenal-Jejunal Bypass Surgery」 Obes Surg 2015. 04.

「Pinealectomy Increases Thermogenesis in Brown Adipocytes and Decreases Lipogenesis in White Adipocytes」 석사학위논문 2016. 06.

「Thyroidectomy stimulates glucagon-like peptide-1 secretion and attenuates hepatic steatosis in high-fat fed rats」 Biochem Biophys Res Commun 2017. 11.

「β-hydroxybutyrate Impedes the Progression of Alzheimer's Disease and Atherosclerosis in ApoE-Deficient Mice」 Nutrients 2020. 02

「Pinealectomy increases thermogenesis and decreases lipogenesis」 Mol Med Rep 2020. 11.

「Tongqiaohuoxue Hinders Development and Progression of Atherosclerosis: A Possible Role in Alzheimer's Disease」 Biology (Basel) 2020. 10.

「Duodenal-jejunal bypass maintains hepatic S-adenosylmethionine/ S-homocysteine ratio in diet-induced obese rats」 Surg Obes Relat Dis 2021. 07.

「Silencing CDCA8 Suppresses Hepatocellular Carcinoma Growth and Stemness via Restoration of ATF3 Tumor Suppressor and Inactivation of AKT/β-Catenin Signaling」 Cancers (Basel) 2021. 03.

「The FGFR Family Inhibitor AZD4547 Exerts an Antitumor Effect in Ovarian Cancer Cells」 Int J Mol Sci 2021. 10.

「Antiviral Activities of High Energy E-Beam Induced Copper Nanoparticles against H1N1 Influenza Virus」 Nanomaterials (Basel) 2022. 01.